1 **Projected future changes in cryosphere and hydrology of a mountainous**

2 **catchment in the Upper Heihe River, China**

4 Zehua Chang [1], Hongkai Gao [1]*, Leilei Yong [1], Kang Wang [1], Rensheng Chen [2],

5 Chuntan Han [2], Otgonbayar Demberel [3], Batsuren Dorjsuren [4], Shugui Hou [5], Zheng

6 Duan [6]

7 [1] Key Laboratory of Geographic Information Science (Ministry of Education of

8 China), School of Geographical Sciences, East China Normal University, Shanghai,

9 China

10 [2] Qilian Alpine Ecology and Hydrology Research Station, Key Laboratory of

11 Ecohydrology of Inland River Basin, Northwest Institute of Eco-Environment and

12 Resources, Chinese Academy of Sciences, Lanzhou 730000, China

13 [3] Department of Geography and Geology Khovd branch of National University of

14 Mongolia, Erkh choloonii street, Khovd, Mongolia

15 [4] Department of Environment and Forest Engineering, National University of

16 Mongolia, Ulaanbaatar 210646, 84140, Mongolia

17 [5] School of Oceanography (SOO), Shanghai Jiao Tong University (SJTU), Shanghai,

18 China

19 [6] Department of Physical Geography and Ecosystem Science, Lund University,

20 Sölvegatan 12, SE-223 62, Lund, Sweden

21 *Correspondence: Hongkai Gao (hkgao@geo.ecnu.edu.cn)

23 **Abstract:** Climate warming exacerbates the degradation of the mountain cryosphere,

24 including glacier retreat, permafrost degradation and snow cover reduction. These

changes dramatically alter the local and downstream hydrological regime, posing

significant threats to basin-scale water resource management and sustainable

development. However, this issue is still not adequately addressed, particularly in

mountainous catchments. We developed an integrated cryospheric-hydrologic model,

FLEX-Cryo model, to comprehensively consider glaciers, snow cover, frozen soil, and

their dynamic impacts on hydrological processes. Taking the mountainous Hulu

catchment located in the Upper Heihe river of China as a case, we utilized the state-of-

the-art climate change projection data under two scenarios (SSP2-4.5 and SSP5-8.5)

from the sixth phase of the Coupled Model Intercomparison Project (CMIP6) to

simulate the future changes in the mountainous cryosphere and their impacts on

hydrology. Our findings showed that under the medium (SSP2-4.5) and high emission

scenario (SSP5-8.5), by the end of the 21st century, the glacier will completely melt out

around the years 2051 and 2045, respectively. The annual maximum snow water

equivalent is projected to decrease by 41.4% and 46.0%, while the duration of snow

cover will be reduced by approximately 45 and 70 days. The freeze onset of seasonally

frozen soil is expected to be delayed by 10 and 22 days, while the thaw onset of

permafrost is likely to advance by 19 and 32 days. Moreover, the maximum freeze depth

of seasonally frozen soil is projected to decrease by 5.2 and 10.9 cm per decade, and

the depth of the active layer will increase by 8.2 and 15.5 cm per decade. Regarding

hydrology, catchment total runoff exhibits a decreasing trend and the tipping point of

glacier runoff occur approximately between 2019 and 2021. Permafrost degradation

will likely reduce the duration of low runoff in the early thawing season, the

discontinuous baseflow recession gradually transitions into linear recessions and the

increase of baseflow. Our results highlight the significant changes expected in the

49 mountainous cryosphere and hydrology in the future. These findings enhance our

50 understanding of cold-region hydrological processes and have the potential to assist

51 local and downstream water resource management in addressing the challenges posed

52 by climate change.

53 **Keywords:** Glacier, Snow cover, Seasonally frozen soil, Permafrost, Runoff, Model

54 prediction

55 1. **Introduction**

56 "How will cold region runoff and groundwater change in a warmer climate?" was

57 identified by the International Association of Hydrological Sciences (IAHS) as one of

58 the 23 unsolved scientific problems (Blöschl et al., 2019). The mountain cryosphere,

59 which includes glaciers, snow cover, and frozen soil in high-altitude regions, has a

60 significant impact on water resources (Adler et al., 2019; Arendt et al., 2020; Rasul et

61 al., 2020; Zhang et al., 2022). The mountain cryosphere is considered a crucial "water

62 tower" and a climate change indicator due to its sensitivity to climate change (Tang et

63 al., 2023). However, the cryosphere is rapidly retreating in many parts of the world,

64 including glacier retreat, expansion of glacier lakes, northward movement of the

65 permafrost southern limit, and shrinking snow cover area (Moreno et al., 2022; S. Wang

66 et al., 2022; Ding et al., 2019; Wang et al., 2023). These changes have disrupted the

67 water tower region and pose significant challenges to sustainable water resources

68 management (Ragettli et al., 2016; Yao et al., 2022).

69 The degradation of the mountain cryosphere varies from region to region

70 (Andrianaki et al., 2019; Wang et al., 2019). Lower altitudes experience a decreasing

71 trend in snow cover days, snow depth, snow water equivalent, and snowmelt due to

72 climate warming, while higher altitudes present a more complex picture (Connon et al.,

73   2021; Nury et al., 2022; Yang et al., 2022). Global continental glacier mass balance

74   from 2006 to 2015 was approximately -123±24 GT yr^{-1}, with significant losses

75   observed in the Southern Andes, Caucasus Mountains, and Central Europe, while the

76   Karakoram and Pamir regions exhibited lesser loss (Intergovernmental Panel on

77   Climate Change (IPCC), 2022; Van Der Geest and Van Den Berg, 2021). Future

78   projections suggest a 40% decrease in global permafrost by the end of the century,

79   potentially transitioning into seasonally frozen soil (Chadburn et al., 2017; Martin et al.,

80   2023). The mountain cryosphere serves as a significant freshwater reservoir, impacting

81   water resources and the hydrological cycle (Ding et al., 2020).

82   In a warming climate, glacier runoff exhibits a "tipping point" characterized by an

83   initial increase followed by a subsequent decline (Rosier et al., 2021; Zhang et al., 2012).

84   While small glaciers have already experienced this tipping point, its occurrence in large

85   glaciers remains uncertain (Brovkin et al., 2021; Huss and Hock, 2018). Permafrost

86   degradation leads to an increase in active layer thickness, resulting in the melting of

87   subsurface ice and an augmentation of soil water storage capacity (Abdelhamed et al.,

88   2022). Additionally, the degradation of the cryosphere significantly impacts the

89   atmosphere, biosphere, surface energy balance, ecological water use, and ecosystems

90   (Gilg et al., 2012; Miner et al., 2022; Pothula and Adams, 2022). Understanding the

91   complex interactions between cryosphere degradation and ecosystems is crucial, but

92   quantitatively observing the degradation process in high-altitude regions is challenging.

93   Hydrological models provide an effective approach to analyze degradation patterns and

94   assess the impact on future water resources (Han and Menzel, 2022).

95   Glacio-hydrology is influenced by both glacier melt and glacier dynamics. Glacier

96   melting models can be categorized into three types: energy balance, temperature index,

97   and hybrid models (He et al., 2021; Gao et al., 2021; Negi et al., 2022; Zekollari et al.,

98   2022). While energy balance models analyze glacier accumulation and melt processes

99   based on solid physical mechanisms, they require extensive forcing data that may not

100 be readily available in mountainous regions (Huss et al., 2010). In contrast, temperature

101 index models are simpler and more effective, requiring fewer parameters (including

102 degree-day factor and threshold temperature) and forcing data (temperature and

103 precipitation) (Bolibar et al., 2022; Vincent and Thibert, 2023). These models perform

104 well at both daily and monthly scales. Glaciers move slowly due to the combined effects

105 of gravity and high viscosity of ice. Due to climate change, ice becomes thinner, and

106 glacier loses its mass balance, which will cause the glacier morphology to evolve to a

107 new balance status. Glacier dynamic models, with full-Stokes approach as the most

108 complete form, and many other simplifications, such as the shallow-ice approximation,

109 and the shallow-shelf approximation, are still computationally expensive, hindering

110 their implications in large scale studies. Three conceptual models are commonly used

111 for glacier evolution: volume-area scaling (V-A) method, accumulation area ratio (AAR)

112 method, and Δh-parameterization (Michel et al., 2022; Wiersma et al., 2022). The first

113 two approaches do not consider the detailed changes in different elevation bands, while

114 the Δh-parameterization approaches only require glacier mass balance as forcing data

115 to analyze changes in ice thickness at different elevation bands based on the relationship

116 between glacier mass balance and glacier area (Huss et al., 2010). The temperature

117 index method coupled with the Δh-parameterization approach serves as an effective

118 module to simulate glacier evolution and its impacts on hydrology.

119 Permafrost hydrology models can be classified into one-dimensional models and

120 distributed watershed models (Elshamy et al., 2020). One-dimensional hydrological

121   models, such as the Stefan equation, the temperature at the top of permafrost (TTOP)

122   model, CoupModel, and SHAW model, are effective in simulating freeze depth,

123   hydrothermal transport, and carbon or nitrogen transport, but they are unable to capture

124   the broader impact of permafrost on hydrology at catchment scale (Kaplan Pastíriková

125   et al., 2023; Li et al., 2022; Liu et al., 2023). On the other hand, distributed watershed

126   models, such as the Cold Regions Hydrological Model (CRHM), Hydrogeosphere

127   (HGS), and Distributed water-heat coupled model (DWHC), consider the spatial

128   variability of permafrost properties and simulate the interactions between permafrost,

129   surface water, and groundwater (Chen et al., 2008; He et al., 2023; Pomeroy et al.,

130   2022). These models operate on a small-scale basis and require extensive prior

131   knowledge, following a "bottom-up" approach that relies on small-scale field

132   observations and situational models to comprehend the effects of permafrost on

133   hydrology (Peng et al., 2016). However, the freeze-thaw cycle is influenced by multiple

134   interconnected factors, including climate, topography, slope orientation, snowpack, and

135   vegetation (Chang et al., 2022). The process of upscaling would lead to the neglect of

136   some variables and the amplification of others (Fenicia and McDonnell, 2022). In

137   contrast, the FLEX-Cryo model is based on the FLEX-Topo-FS model, which employs

138   a "top-down" modeling procedure that involves observed data analysis, qualitative

139   perceptual modeling, quantitative conceptual modeling, and the testing of model

140   realism. This model exhibits the ability to accurately and expeditiously identify key

141   elements in permafrost hydrological processes and then simulate hydrology at the

142   catchment scale (Beven., 2012; Gao et al., 2022).

143   The aim of this study is to integrate the FLEX-Topo-FS model and a glacier

144   evolution model (Δh-parameterization) to develop a landscape-based model of the

145   mountain cryosphere, referred to as FLEX-Cryo. This model will be utilized to simulate

146   changes in various components of the mountain cryosphere and evaluate their impacts

147   on hydrological processes, thereby enhancing our understanding of the hydrological

148   cycle. The model will be driven by eight bias-corrected Global Climate Models (GCMs)

149   under SSP2-4.5 and SSP5-8.5 scenarios obtained from the Coupled Model

150   Intercomparison Project Phase 6 (CMIP6), which will be used to predict future changes

151   in glaciers, snow, and frozen soil, as well as their effects on hydrology.

152   **2.Study area and data**

153   **2.1 Study area**

154   The Hulu catchment is located in the upper reaches of Heihe River basin (38°12′

155   N-38°17′ N, 99°50′ E-99°53′ E) and about 23.1 km^2. The elevation ranges

156   from 2960-4820m. The Hulu catchment belongs to continental monsoon climate.

157   Rainfall is the major phase of precipitation, and there is also snowfall in the winter.

158   Four landscapes are identified, i.e. glacier (5.6%), alpine desert (53.5%), vegetation

159   hillslope (37.5%), and riparian zone (3.4%; Fig.1 (c)). The landscape pattern in Hulu

160   catchment has typical altitude zonality. The vegetation and riparian are almost

161   distributed in the lower elevation bands. Alpine desert, and glacier are in the high

162   elevation bands. There is almost no human activity in the catchment (Liu and Chen,

163   2016; Li et al., 2014). There are two major glaciers, i.e. Glacier1 and Glacier2 (Fig.1

164   (b) and Fig.2) in the catchment. And the Galcier1 was also named as the Shiyi Glacier

165   in the glacier catalogue of China. Seasonally frozen soil and permafrost both exist in

166   the catchment. The lower limit of permafrost is around in 3650-3700 m. Permafrost

167   region account for 64% of the total catchment and the others are seasonally frozen soil.

168   The soil generally starts to freeze in the October (Gao et al., 2019). Thus October 1 was

169   set as the start of hydrological year, so forth. All the interannual variations in this study

170   were based on the hydrology year.

171
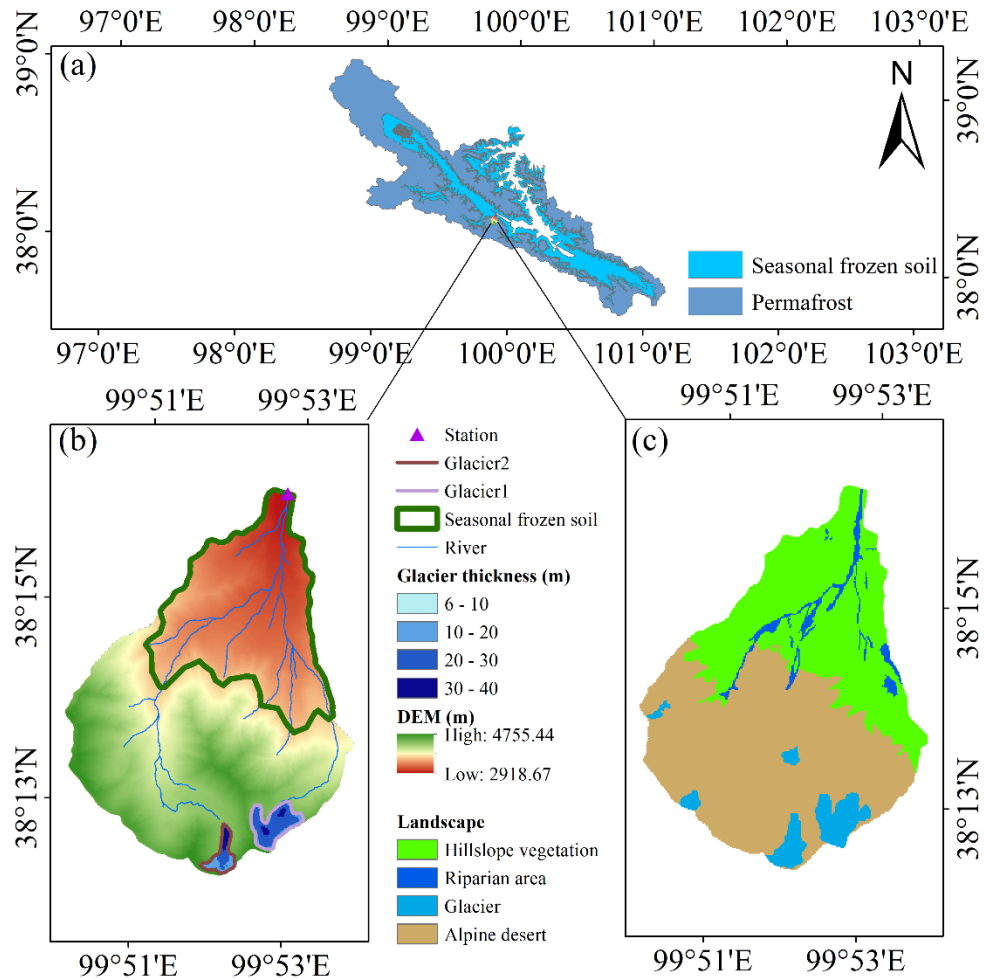
172

173   Figure 1. (a) The distribution of permafrost and seasonally frozen soil on the

174   upper Heihe River basin, and the location of Hulu catchment. (b) The digital elevation

175   model and the thickness of the two major glaciers. (c) Spatial distribution of four

176   landscapes (glacier, alpine desert, vegetation hillslope, and riparian zone)
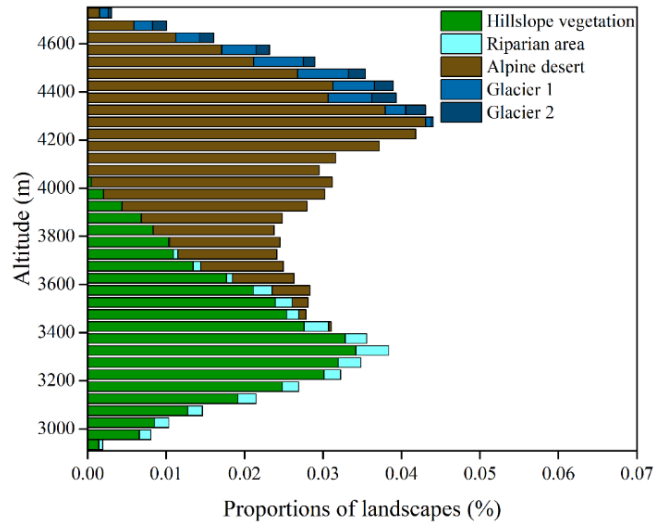
Figure 2. Landscape classification at different elevation bands

2.2 Data

Temperature and precipitation are observed at 2920 m, near the outlet of the catchment, from 2011 to 2014. Farinotti et al. (2019) used five models which used the ice flow dynamics to invert ice thickness from surface features to estimate the ice thickness distribution of about 21500 glaciers outside the Greenland and Antarctic ice sheets. We used the estimated data for the initial thickness distribution of Glacier1 and Glacier2 (data downloaded from https://doi.org/10.3929/ethz-b-000315707).

The Couple Model Intercomparison Project phase 6 (CMIP6) is widely used to predict future climate. Eight general circulation models (GCMs) (Table 1) under two climate scenarios (SSP2-4.5 and SSP5-8.5) are used for predicting future climate. The selected models have been well validated at the nearby catchments (Xing et al., 2023; Yin et al., 2021; Ma et al., 2022; Zhu and Yang, 2020; Chen et al., 2022). SSP2-4.5 scenario represents medium part of the future pathways, which is usually a referenced experiment comparing others CMIP6-Endorsed MIPs and it produces a radiative forcing of 4.5 W m^{-2} in 2100. SSP5-8.5 scenario represents the high emission scenario and it produce a radiative forcing of 8.5 W m^{-2} in 2100.

195   Although the reliability of GCMs has been verified in the previous studies, there

196 is certain bias in the output that needs to be corrected. Firstly, outputs from eight GCMs

197 under two climate scenarios are interpolated to 0.5°×0.5°, then the bias corrects are

198 carried out by CMhyd software (download from

199 https://swat.tamu.edu/software/cmhyd/) in which four methods were used including:

200 distribution mapping of precipitation and temperature, linear scaling of precipitation

201 and temperature, variance scaling of temperature and local intensity scaling (LOCI) of

202 precipitation (Teutschbein and Seibert, 2012). The bias-corrected precipitation and

203 temperature were calculated by using the equal weighted average method to obtain the

204 multi-model ensemble average values under the SSP2-4.5 and SSP5-8.5 scenarios,

205 which reduce the uncertainty caused by a single bias correction method and a single

206 GCM, the method is described as follow:

207
$$P_{\text{ave}} = \frac{1}{N_{GCM}} \left(\sum_{j=1}^{N_{GCM}} \left(\frac{1}{N_{bias}} \left(\sum_{i=1}^{N_{bias}} (P_i) \right) \right) \right) \quad (1)$$

208 Where the P_{ave} is the average value of the multi-model and multi -method, P_i is the

209 projected climate data of an GCM, N_{bias} is the number of correction methods (N_{bias} is 3

210 in this research) and N_{GCM} is the number of GCM (N_{GCM} is 8 in this research).

211 Table 1. Details of data from eight GCMs used in this study

GCM	Institutions	Grid	Lon. × Lat.
ACCESS-CM2	Australian Community Climate and Earth System Simulator	192×144	1.875°×1.250°
ACCESS-ESM1-5	Australian Community Climate and Earth System Simulator	192×144	1.875°×1.250°
BCC-ECM1	Beijing climate center	320×160	1.125°×1.125°
CMCC-CM2-SR5	Fondazione Centro Euro-	288×192	1.25°×0.938°

	Mediterraneo sui Cambiamenti Climatici		
CMCC-ESM2	Fondazione Centro Euro-Mediterraneo sui Cambiamenti Climatici,	288×192	1.25°×0.938°
GFDL-CM4	National Oceanic and Atmospheric Administration	144×90	2.5°×2°
MPI-ESM1-2-LR	Max Planck Institute for Meteorology	192×96	1.875°×1.875°
NESM3	Nanjing University of Information Science and Technology	192×96	1.875°×1.875°

212 **3.Methodology**

213 **3.1 FLEX-Cryo model**

214   The FLEX-Cryo model is a landscape-based cryospheric hydrological model that

215 considers multiple elements of cryosphere and their impacts on hydrology, including

216 glacier, snow and frozen soil. Figure 3 shows the structure of the FLEX-Cryo model.

217   The model parameters used in this research were obtained the optimal parameter

218 set from a previous study conducted in the same catchment (Gao et al., 2022). The

219 selected parameters are listed in Table 2 and the other variables in calculating (Fig. 3)

220 are listed in Table 4.

221 Table 2. Model parameters and their values in this study

Parameter	Name	Parameter value
F_{dd} (mm°C^{-1}d^{-1})	Snow degree day factor	3.10
C_g (-)	Glacier degree factor multiplier	2.27
S_{umax_V} (mm)	Root zone storage in vegetation hillslope	100.32
S_{umax_D} (mm)	Root zone storage in alpine desert	20.63
S_{umax_R} (mm)	Root zone storage in riparian wetland	20.26
β (-)	The shape of storage capacity curve	0.11

C_e (-)	Soil moisture threshold for reduction of evaporation	0.50
D (-)	Splitter to fast and slow response reservoirs	0.20
T_{lagf} (days)	Lag time from rainfall to peak flow	2.00
K_f (days)	Fast recession coefficient	1.65
K_s (days)	Slow recession coefficient	79.09
k (W (m K)$^{-1}$)	Thermal conductivity	2.00
ω (-)	Water content as a decimal fraction of the dry soil weight	0.12
ρ(kg/m^3)	Bulk density of the soil	1000
Pcalt (%/100m)	Precipitation increasing rate	4.20
Tcalt (℃/100m)	Temperature lapse rate	0.68

222 **3.1.1 Glacier and snow melting**

223 The threshold temperature (T_t) determines the phase of precipitation, i.e. snowfall

224 or rainfall. Snow reservoir (S_w) accounts for the snow accumulating, melting (M_w) and

225 water balance(Eq. 9). The number of days when S_w is non-zero represent the snow cover

226 days and the maximum S_w is the maximum snow water equivalent of a year (Giovando,

227 J. and Niemann, J. D., 2022). Both Glacier and snow melt were calculated by the

228 temperature index method, which is on basis of the degree-day factor (F_{dd}). If there is

229 no s'ow cover, the glacier starts to melt. Due to the lower albedo, the degree-day factor

230 of ice is greater than that of snow cover, and is multiplied by a coefficient C_g to calculate

231 glacier melt (Eq. 14).

232 **3.1.2 Rainfall-runoff module**

233 The rainfall and snow melt enter the root zone reservoir S_u, then runoff (R_U)

234 generates based on the input water and the relative root zone soil moisture (S_u/S_{umax})

235 and the shape of root zone storage capacity distribution determined by parameter β (Eq.

236 16). Actual evaporation E_a is also estimated based on the soil moisture S_u/S_{umax} and the

237   potential evaporation by Hamon equation (Hamon, 1961). The generated runoff (R_U) is

238   separated, by parameter D, into two linear reservoirs, i.e. the fast response reservoir (S_f)

239   and slow response reservoir (S_s) (Eq. 18 and 19). The two reservoirs are respectively

240   controlled by fast recession parameter K_f and slow recession parameter K_s to simulate

241   the subsurface storm flow Q_f and groundwater runoff Q_s (Eq. 7,8).

242   Different landscapes, for example, alpine desert, vegetation hillslope and riparian

243   zone, have different sizes of root zone storage capacity (S_{umax}) (Aubry-Wake et al.,

244   2023). In the vegetation hillslope, plants have well-developed root systems and the root

245   zone has a larger storage capacity. Therefore, the S_{umax_V} was set to a larger value. For

246   the alpine desert and riparian zone, the S_{umax_D} and S_{umax_R} were both limited due to the

247   less developed root system and storage capacity.

248   **3.2 Frozen soil module**

249   The Stefan equation was employed to estimate freeze (thaw) depth. This equation

250   is calculated by the freeze (thaw) index (F), which neglects the sensible heat. The

251   equation is as follows:

252
$$\varepsilon = \left(\frac{2 \cdot 86400 \cdot k \cdot F}{L \cdot \omega \cdot \rho}\right)^{0.5} \quad (2)$$

253   where, the ε is the freeze / thaw depth (m), k is the thermal conductivity (2 W (m

254   K)$^{-1}$), F is the freeze/ thaw index(℃), Q_L is the volumetric latent heat of soil (J m^{-3}), L

255   is the latent heat of the fusion of ice (3.35×10^5 J kg^{-1}), ω is the water content as a

256   decimal fraction of the dry soil weight (0.12), and ρ is the bulk density of the soil

257   (1000 kg m^{-3}).

258   Since the Stefan equation requires ground surface temperature, which is difficult

259   to measure and often lacks data. During freezing, the air temperature was translated into

260   ground temperature by multiplier 0.6 and the ground temperature was the same as the

261 air temperature during thawing (Gisnås et al., 2016). In this research, the freeze-thaw

262 process was simulated at each Hydrologic Response Unit (RHU) by the Stefan equation

263 driven by distributed air temperature. The lower limit of permafrost was also estimated

264 by the distributed soil freeze index and thaw index where the freeze index is equal to

265 the thaw index in the mountain region.

266   In the freezing and frozen season, there is no runoff generated due to precipitation

267 in the form of snowfall and the soil being frozen. During this period, runoff only comes

268 from the groundwater of the supra-permafrost and no runoff (R_U) is generated from root

269 zone reservoir to the fast response reservoir (S_f) and slow response reservoir (Ss).

270 Therefore, we set the R_U is zero in this season. In the freezing season, when the freezing

271 depth is less than 3 m, the groundwater discharge in the supra-permafrost is still

272 connected, which can be simulated with a linear groundwater reservoir (S_s) and the slow

273 recession coefficient (K_s). When the freezing depth is greater than 3 m at a Hydrologic

274 Response Unit, the groundwater is frozen and there is little runoff generated from the

275 groundwater discharge at the Hydrologic Response Unit. So, in the FLEX-Cryo model,

276 the groundwater reservoir (S_s) was reduced to 10% of its storage to represent the

277 groundwater being frozen (Eq. 3,4). The other 90% of the storage water was frozen in

278 the groundwater system (Eq. 4). In the model, the soil begins to freeze from high

279 elevation to the lower elevation, which affects the groundwater. The groundwater

280 reservoir freezes along the elevation, stopping the function of a series of cascade

281 groundwater buckets, which is the key reason for discontinue recession.

282   In the thawing season, the freeze statue at the lowest elevation controls the

283 hydraulic connectivity between groundwater system and soil. If the freeze depth is

284 larger than thaw depth calculated by the Stefan equation, the soil is still frozen and the

285 connectivity between groundwater system and soil is still closed. There is no runoff

286 generated (*Ru*) but the root soil moisture (*Su*) accumulates and evaporation is the only

287 outflow from the root zone. Once the thaw depth is larger than the freeze depth, the

288 frozen groundwater reservoir is released to the groundwater discharge (Eq. 4).

289 Complete thawing at the lowest elevation represents the end of the thawing season and

290 the start of completely thawed season. In the completely thawed season, the

291 groundwater and soil are connected and not affected by the frozen soil.

292 $$\frac{dS_s}{dt} = R_s - Q_s - F_s \quad (3)$$

293 $$F_s = \begin{cases} 0.9 \cdot S_s & freeze\ depth\ (\varepsilon) \geq 3\ m \\ -0.9 \cdot S_s & once\ thaw\ depth\ reach\ to\ yearly\ \max \\ & or\ thaw\ depth\ \geq thaw\ depth \end{cases} \quad (4)$$

294 **3.3 Δh-parameterization**

295   The Δh-parameterization is a mass conservation method to assess the change of

296 ice-covered, glacier length and glacier thickness in response to global warming. The

297 glacier mass balance (GMB) calculated by FLEX-Cryo was redistributed to glacier

298 elevation bands. It is an observed truth that the lower elevation bands loss more ice than

299 higher elevation bands. The lost ice volume, calculated by a mass balance model, is

300 converted into a distributed ice thickness change according to the Δh-parameterization.

301 (Gao et al., 2021; Huss et al., 2010).

302   The Δh-parameterization method was employed, which relies on empirical curves

303 that are dependent on the size of the glacier. The study categorized glaciers into three

304 size classes: large valley glacier (area > 20 km^2), medium valley glaciers (5 km^2 < area

305 < 20 km^2), and small glaciers (area < 5 km^2). Both Glacier1 and Glacier2 had areas less

306 than 5 km^2, and categorized as small glaciers. The small glacier equation in this study

307 is as follows:

308    $$\Delta h = (h_r - 0.30)^2 + 0.60(h_r - 0.30) + 0.09 \quad (5)$$

309   Where, $\varDelta h$ is normalized surface elevation change and h_r is the normalized

310   elevation range. Based on this equation, the glacier elevation and surface area were

311   evolved every 5 years to avoid the circumstance of glacier advancing. The

312   corresponding glacier melting HRU was transformed into alpine desert (Wei et al.,

313   2023).

314

315   Table 3. The FLEX-Cryo model equations

Landscape	Runoff equation	Water balance equation	Structural equation
Glacier	$Q_g = \dfrac{S_g}{K_{f,g}}$ (6)	$\dfrac{dS_g}{dt} = P_l + M_g - Q_g$ (9)	$M_g = \begin{cases} F_{dd} \cdot T \cdot C_g & S_w \text{ and } T > 0 \\ 0 & S_w \text{ and } T > 0 \end{cases}$ (14)
Alpine desert Hillslope vegetation Riparian area	$Q_f = \dfrac{S_f}{K_f}$ (7) $Q_s = \dfrac{S_s}{K_s}$ (8)	$\dfrac{dS_w}{dt} = P - M_W$ (10) $\dfrac{dS_u}{dt} = P_l + M_W - E_a$ $\qquad\qquad - R_u$ (10) $\dfrac{dS_f}{dt} = R_f - Q_f$ (12) $\dfrac{dS_s}{dt} = R_s - Q_s$ (13)	$M_w = \begin{cases} F_{dd} \cdot T & T > 0 \\ 0 & T > 0 \end{cases}$ (15) $R_u = (P_l + M_w) \cdot \left(1 - \left(1 - \dfrac{S_u}{S_{umax}}\right)^\beta\right)$ (16) $E_a = E_p \cdot \left(\dfrac{S_u}{C_e \cdot S_{umax}}\right)$ (17) $R_f = R_u \cdot D$ (18) $R_s = R_u \cdot (1 - D)$ (19) $R_{fl}(t) = \sum_{i=1}^{T_{lagf}} cf(i) \cdot R_f(t - i + 1)$ (20) $cf(i) = i / \sum_{u=1}^{T_{lagf}} u$ (21)

316   **3.4 Spatial discretization of the catchment**

317   The catchment area was divided into 37 elevation bands ranging from 2960 m to

318   4820 m, with an interval of 50 m. These elevation bands were classified based on four

319   landscapes: glacier, alpine desert, vegetation hillslope, and riparian zone (Fig. 2 and Fig.

320   3). As a result, there were a total of 148 Hydrologic Response Units (HRUs) in the

321   catchment. The landscape of alpine desert was the most widespread, covering an

322   elevation range of 3425 m to 4727 m. The glacier was found in higher altitude areas,

323   specifically between the elevation bands of 3725 m and 4727 m.
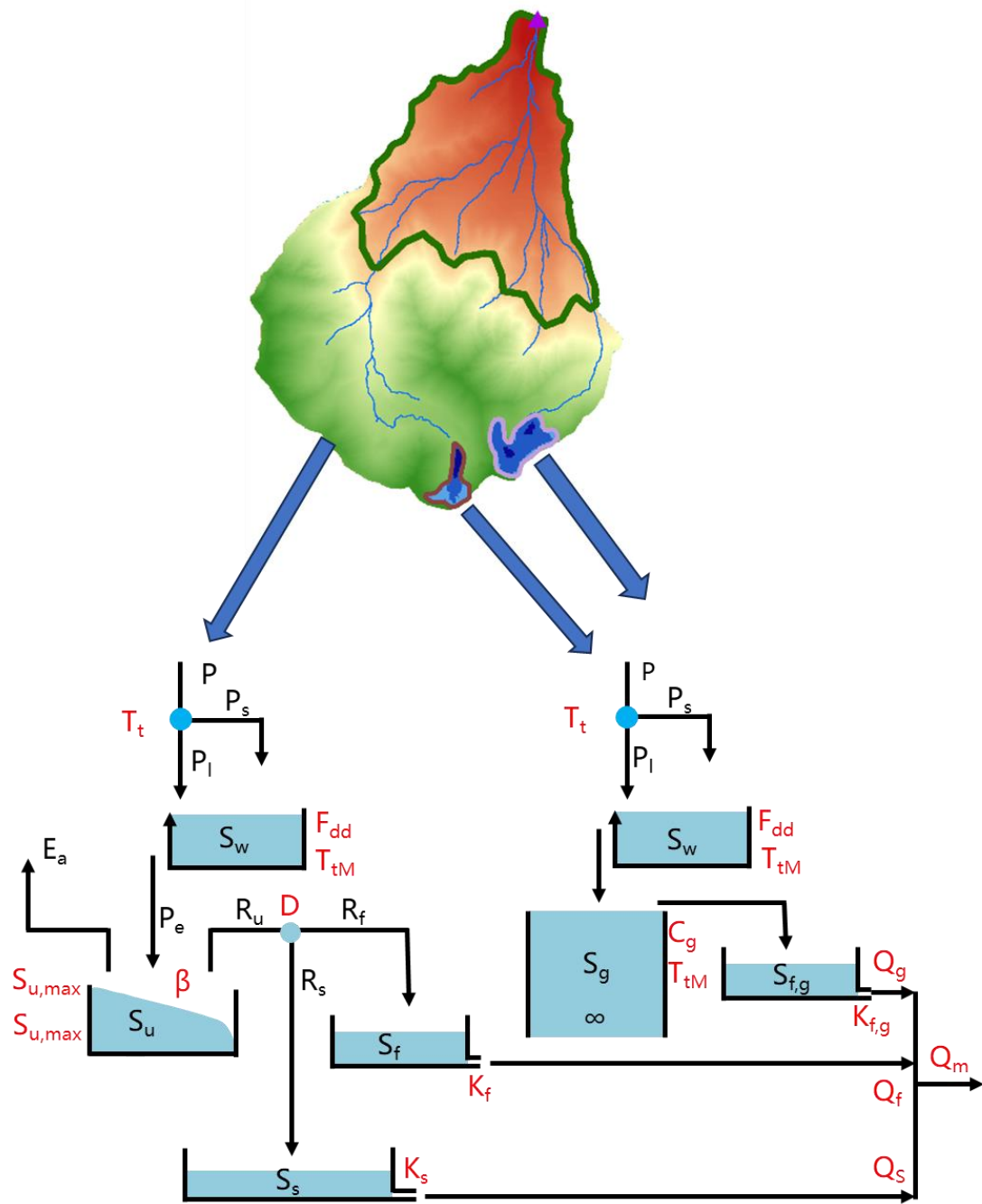
324

325   Figure.3 Structure of the FLEX-Cryo model. The abbreviation in red color indicates

326   paraments and the abbreviations in black indicate storage components and fluxes.

327   Table 4. The variables in Table 3 and Figure 3 and their meaning

Variables	Meaning
P (mm/day)	precipitation
T_t (℃)	Threshold temperature
P_s (mm/day)	Solid precipitation

P_l (mm/day)	Liquid precipitation
S_{wl} (mm)	Liquid water inside the snow pack.
S_w (mm)	Solid snow pack
T_{tM} (℃)	The threshold temperature for snow and glaciers melting
P_e (mm)	Generated runoff to soil/ice surface
E_a (mm)	Actual evaporation
R_u (mm)	water that exceeds the storage capacity
S_f (mm)	Fast flow reservoir
S_s (mm)	Slow flow reservoir
$S_{f,g}$ (mm)	Glacier linear reservoir
Q_f (mm/day)	Subsurface storm flow
Q_s (mm/day)	Groundwater runoff
Q_g (mm/day)	Runoff in glacier region
Q_m (mm/day)	All runoff

3.5 Model evaluation metrics

The Kling–Gupta efficiency (KGE), Nash–Sutcliffe efficiency (NSE), coefficient of correlation (R) and root mean square error (RMSE) were used to comprehensively assess the model performance and the reliability for the model. All The KGE, NSE, R and RMSE are all less than 1. For KGE, NSE and R, values closer to 1 indicate better performance. A lower RMSE value indicates less error and better model performance. These metrics can be calculated as follows:

$$KGE = 1 - \sqrt{(r-1)^2 + (\alpha-1)^2 + (\beta-1)^2} \quad (22)$$

$$NSE = 1 - \frac{\sum_{t=1}^{n}(Q_0 - Q_m)^2}{\sum_{t=1}^{n}(Q_0 - \overline{Q_0})^2} \quad (23)$$

$$RMSE = \sqrt{\frac{1}{N}\sum_{i=1}^{n}(Q_0 - Q_m)^2} \quad (24)$$

$$R = \frac{\sum_{t=1}^{n}(Q_0 - \overline{Q_0})(Q_m - \overline{Q_m})}{\sqrt{\sum_{t=1}^{n}(Q_0 - \overline{Q_0})^2}\sqrt{\sum_{t=1}^{n}(Q_m - \overline{Q_m})^2}} \quad (25)$$

339   where, r is linear correction coefficient between simulation and observation, α is

340   the ratio of the stand deviation of simulated variables and observed variables, β is the

341   ratio of the average value of simulated and observed variables, Q_0 is the observation

342   runoff, $\overline{Q_0}$ is the average observed runoff and Q_m is the simulation runoff.

343   **4. Results**

344   **4.1 Performance of bias correction and runoff depth simulation**

345   **4.1.1 Bias correction performance**

346   The accuracy of climate projection varied with the multiple bias correction method

347   (Fig. 4). The distance between the observation and the projection is inversely

348   proportional to the accuracy. Before the bias correction, the distance is relatively far

349   especially for precipitation indicating that there is a large error between observatiosn

350   and GCMs projection. After the bias correction, the distance diminishes, indicating that

351   the bias correction improves the accuracy, particularly for precipitation.
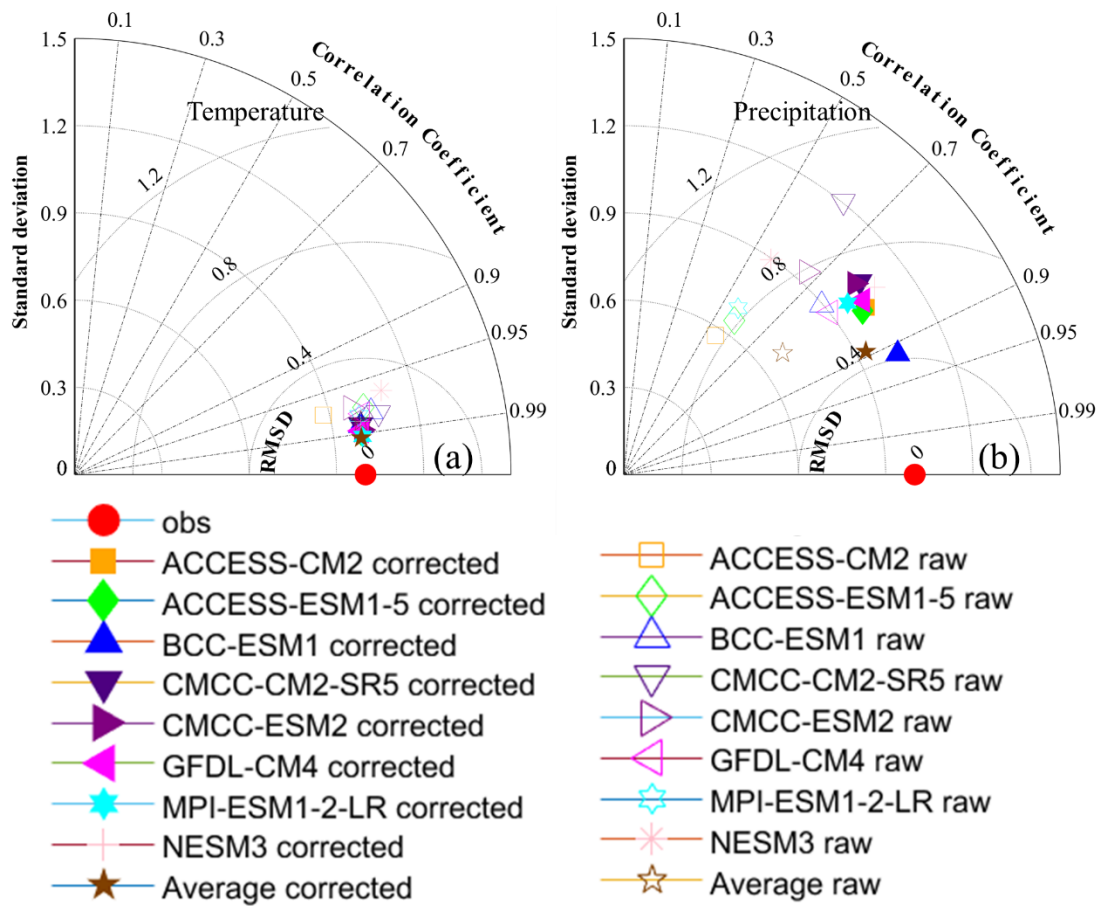
352

353   Figure 4. Taylor diagram of monthly temperature and precipitation simulation. The

354   hollow points are the uncorrected projection, the solid point are the corrected projection

355   and the solid red circle is the reference values (observation).

356   **4.1.2 Performance of runoff simulation**

357   We assessed the performance of the FLEX-Cryo model for runoff simulation based

358   on historical observations. Throughout the entire assessment period, the KGE is 0.83,

359   NSE is 0.73, R is 0.74, and RMSE is 0.77 mm/day. These results indicate that the model

360   can reproduce hydrographs effectively. The good model performance demonstrates the

361   robustness of the FLEX-Cryo model, ensuring accurate estimation of future

362   hydrological changes (Fig. 5).
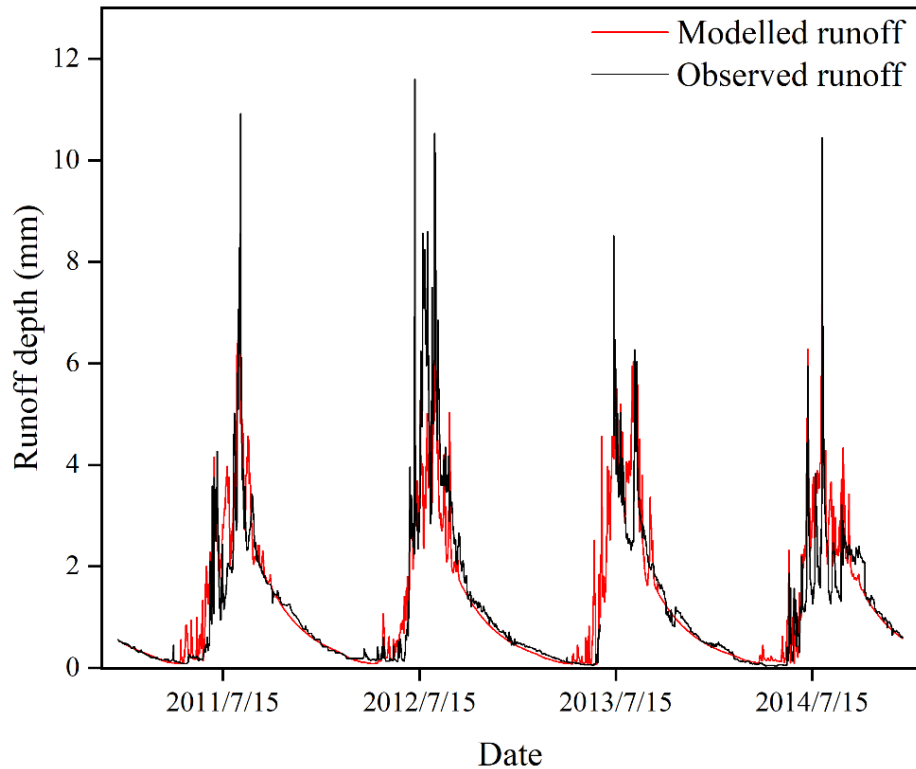
363

364 Figure.5 Simulation results of the FLEX-Cryo model and the comparisons with

365 observation from 2011 to 2014.

4.2 Future climate change

367 Figure 6 shows the prediction of future climate in 2015-2100 under the SSP2-4.5

368 and SSP5-8.5 based on the average values of eight climate models (adjusted for bias).

369 According to the SSP2-4.5, the temperature will increase by 2.07°C relatively steadily

370 by 2100. Under the SSP5-8.5, temperatures are projected to continue to rise by 5.04°C

371 over the course of the century. Precipitation changes are more variable than temperature,

372 especially after the eighties of the 21st century under the SSP5-8.5. Overall, the

373 precipitation under the SSP2-4.5 increased by 14.25 %, and the precipitation increased

374 by 33.50 % under the SSP5-8.5. Before the 2080s, the increase in precipitation was

375 almost the same under different scenarios, about 8.9 mm 10 years^{-1} and 8.5 mm 10

376 years^{-1}, respectively. Although there are some uncertainties associated with temperature

377   and precipitation, the increasing trend of temperature and precipitation are still

378   distinguished, especially for the SSP5-8.5.
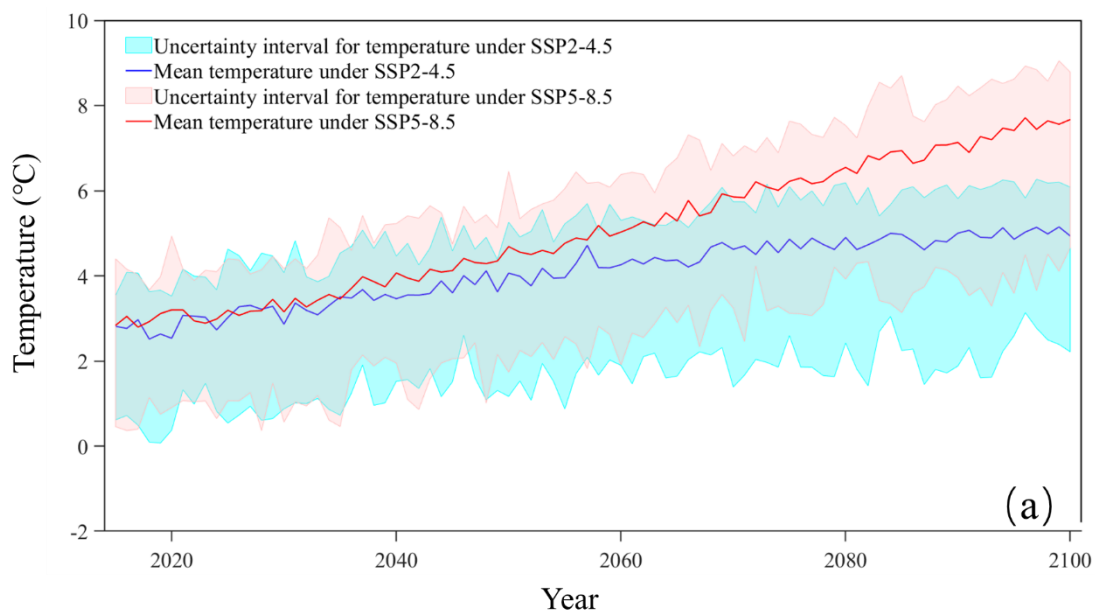
379

380
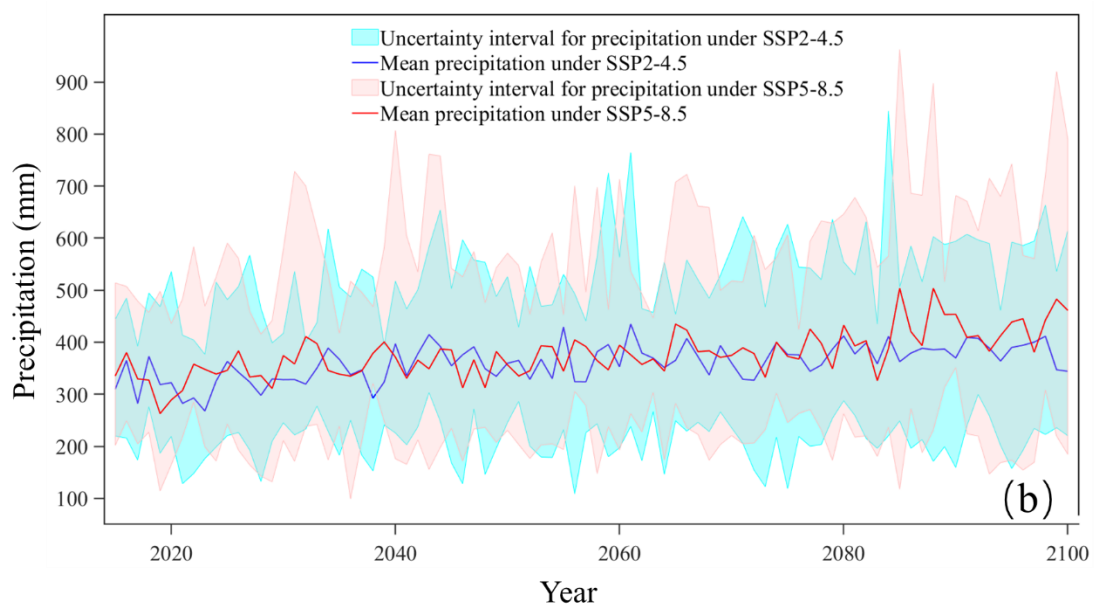
381

382   Figure 6. (a) the annual average temperature and (b) annual precipitation mean of

383   bias adjusted multi-Global Climate Model from 2015-2100. The blue and red areas

384   indicate the uncertainty caused by 8 climate change models of SSP2-4.5 and SSP 5-8.5

385   scenarios.

4.3 The change of cryosphere in the future

4.3.1 Predicting glacier retreat

Figure 7 shows changes in glacier thickness at the highest elevation band and volume for the Glacier 1 and the Glacier 2 under two SSPs from years 2015–2100. Starting from the 2020s, the glacier volume showed a rapid decline, and after the 2030s, the glacier entered a phase of rapid thinning. Around 2040, the glacier degradation reached a stabilization period, during which glaciers were only present in the highest elevation band. According to the SSP2-4.5 scenario, Glacier1 and Glacier2 are projected to completely melt and disappear by 2051 and 2046, respectively. Under the SSP5-8.5 scenario, the complete melt-out time is slightly earlier, occurring in 2045 and 2044 for Glacier1 and Glacier2, respectively. After the glaciers completely melt ablated glacier area will transform into alpine desert.

Taking the glacier changes in 2025, 2035, and 2045 as examples, under the SSP2-4.5 scenario, the area of Glacier1 is projected to decrease to 5.49×105 m^2, 1.52×105 m^2, and 0.26×105 m^2, with corresponding volume reductions to 5.27×10^6 m^3, 1.03×10^6 m^3, and 0.26×10^6 m^3, respectively (Fig. 9). Comparatively, the retreat trend is more pronounced under the SSP5-8.5 scenario. The area of Glacier1 is projected to be 4.00×10^5 m^2, 0.81×10^5 m^2, and 0.26×10^5 m^2, with volumes of 4.86×10^6 m^2, 0.71×10^6 m^3, and 0.03×10^6 m^3, respectively. The degradation of Glacier2 follows a similar pattern to that of Glacier1, except that Glacier2 experiences less ice loss. According to the SSP5-8.5 scenario, Glacier2 is projected to completely melt by 2045. In 2025 and 2035, the area of Glacier2 is 1.67×105 m^2 and 0.51×105 m^2 for both scenarios, respectively. These glaciers are only distributed within the elevation bands from 4625 m to 4727 m and from 4675 m to 4727 m.

410

411
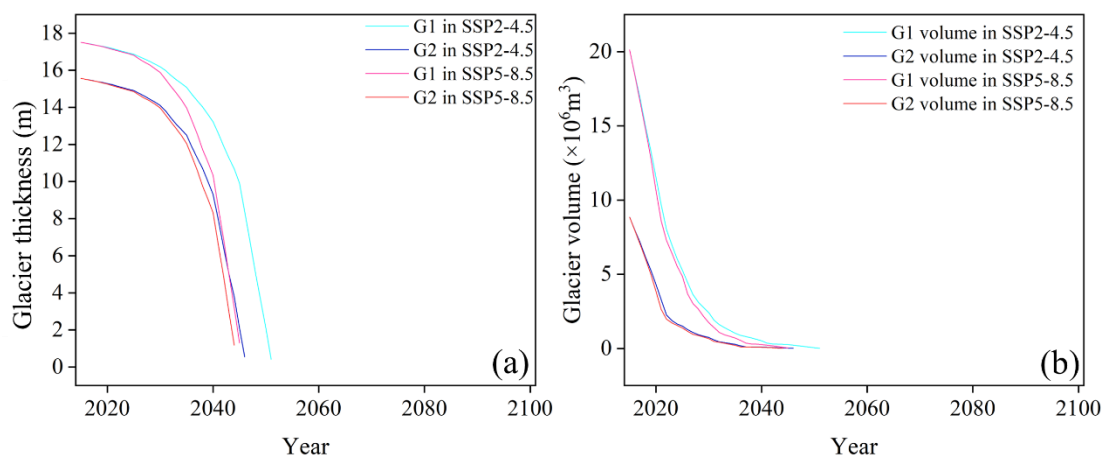
Figure 7. The glacier thickness (a) and glacier volume (b) change from 2015 to 2100 for the Glacier1 and Glacier 2

4.3.2 Forecasting the degradation of frozen soil

The degradation of seasonally frozen soil and permafrost are projected by FLEX-Cryo model. Under SSP2-4.5, by the end of 21st century, the freeze onset of seasonally frozen soil will be delayed by 10 days and the freeze-thaw cycle duration will shorten approximately 1 month. The maximum freeze depth of seasonally frozen soil is expected to decrease by 5.17 cm per decade. The thaw onset of permafrost will be advanced by 19 days and the freeze-thaw cycle duration would increase nearly 50 days. The active layer thickness will rise by approximately 8.24 cm per decade. Meanwhile, the degradation trend of permafrost is more severe under the SSP5-8.5 scenario. Under SSP2-4.5, the freeze onset of seasonally frozen soil will be shortened by 22 days and the freeze-thaw cycle duration will reduce by over 2 months. The thaw onset of permafrost will occur approximately 1 month earlier, and the freeze-thaw cycle duration of permafrost will increase by nearly 3 months. Compared with the SSP2-4.5, the decreasing trend of the maximum freeze depth and the increasing trend of the active

429 layer thickness are approximately twice as pronounced under the SSP5-8.5. By 2100

430 Seasonally frozen soil will begin to freeze around mid-November and late November,

431 while permafrost will start to thaw in mid-May and early June by the year 2100 under

432 two SSPs.

433   Under the SSP2-4.5 and SSP5-8.5, the lower limit of permafrost gradually expands

434 along the altitudinal gradient, with rates of 4.30 m per year and 8.75 m per year,

435 respectively (Fig. 9). In the SSP2-4.5, the lower limit of permafrost is projected to reach

436 altitudes of 3685 m, 3795 m, 3835 m, 3865 m, 3985 m, and 4015 m in the years 2025,

437 2035, 2045, 2055, 2075, and 2095, respectively. The lower limit of permafrost in 2095

438 under the SSP2-4.5 scenario is comparable to the lower limit of permafrost (3965m) in

439 2055 under the SSP5-8.5 scenario. The lower limit is projected to increase to 4355 m

440 by 2095 under the SSP5-8.5 scenario.
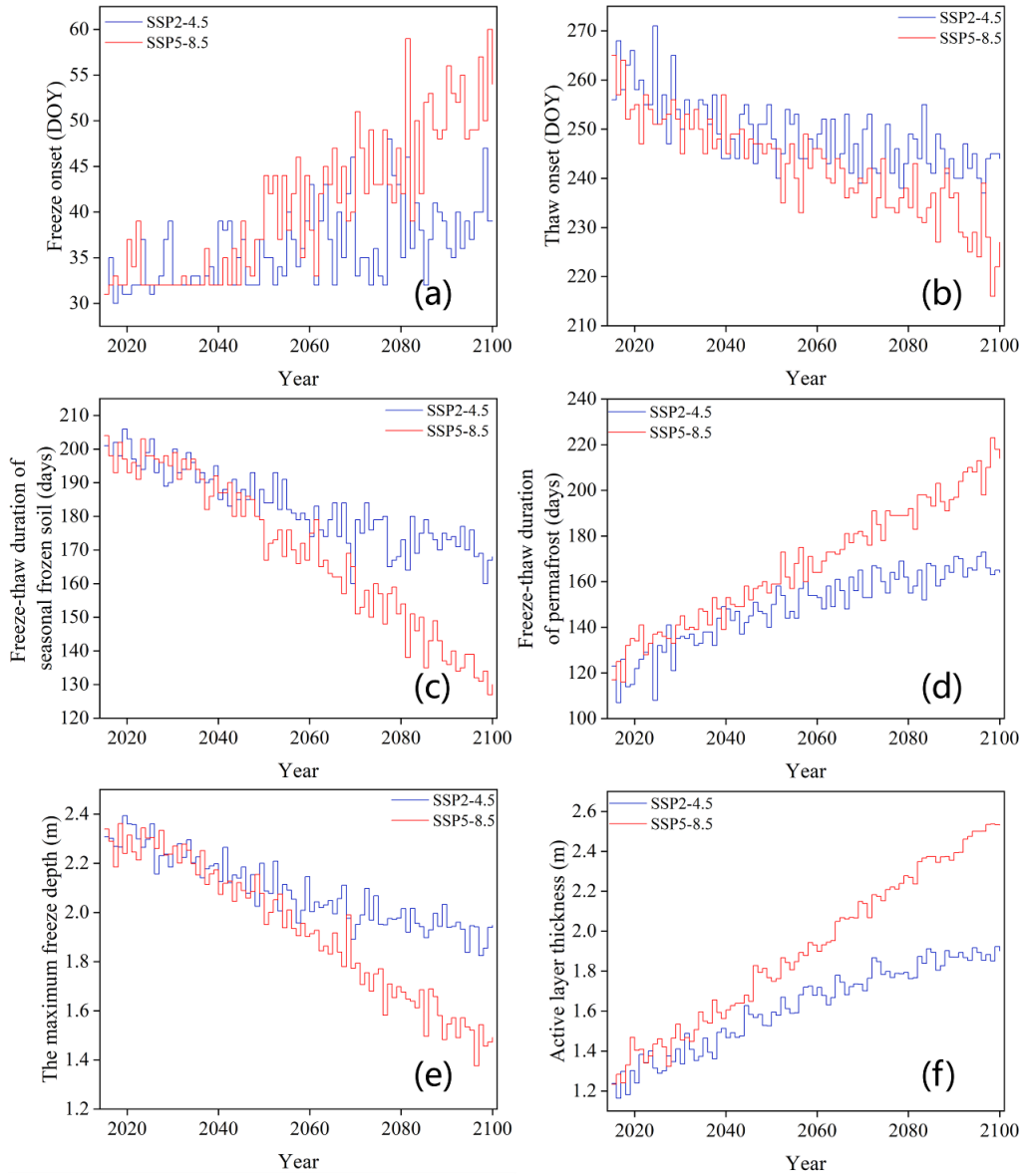
441

442   Figure 8. Changes in seasonally frozen soil and permafrost from 2015-2100 under

443   SSP2-4.5 and SSP5-8.5 scenarios. (a, b) Freeze and thaw onset. (c, d) Freeze-Thaw

444   duration of frozen soil and permafrost. (e, f) The maximum freezing depth and active

445   layer thickness.
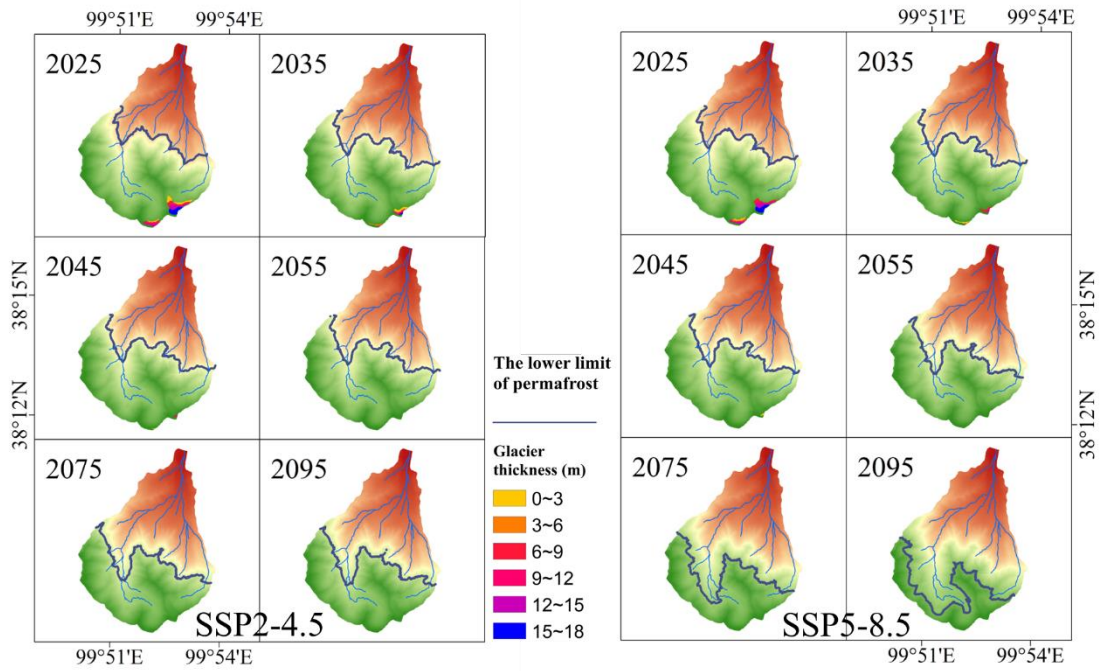
446

447   Figure 9. Changes of ice thickness and the lower limit of permafrost in 2025, 2035,

448   2045, 2055, 2075 and 2095 under SSP2-4.5 and SSP5-8.5.

449   **4.3.3 Snow change in the future**

450   The duration of snow cover is projected to decrease continuously in the future (Fig.

451   10). Under the SSP2-4.5, snow cover days are likely to be shortened by 45 days and

452   snow water equivalent will decrease by 0.24 mm per year. Compared with SSP 2-4.5,

453   snow cover has a more reduction under SSP5-8.5. Under SSP5-8.5, snow cover day is

454   expected to be around 76 days and snow water equivalent will decrease by 0.35 mm

455   per year.

456
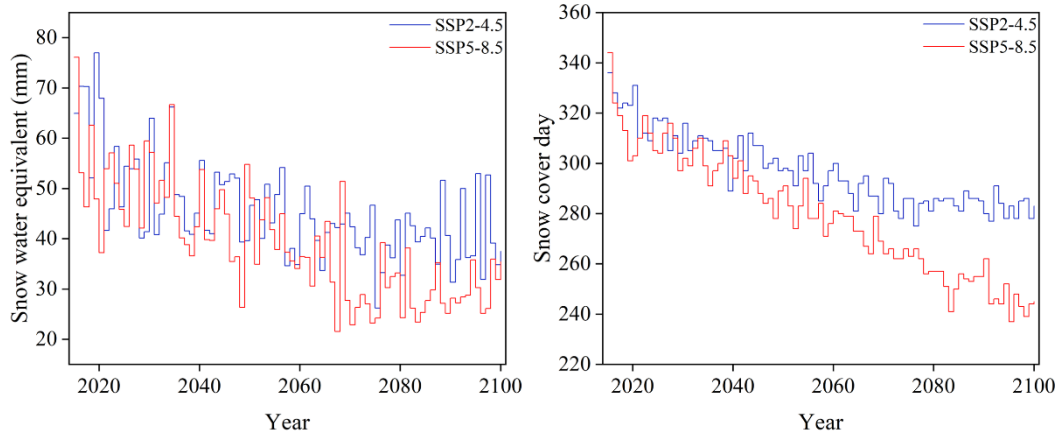
Figure 10. Changes of snow water equivalent and snow cover day from 2015-2100

under SSP2-4.5 and SSP5-8.5.

4.4 Projected future runoff

The runoff in the catchment were predicted by the FLEX-Cryo model under SSP2-4.5 and SSP5-8.5. The tipping point of the glacier melting has already occurred (around 2020). After the turning point, glacier runoff and runoff of the total basin decreases dramatically until glacier completely melt. Then the runoff of the total basin will moderate increase. After glacier completely melt, runoff of the total basin would decrease by 15.56% and 18.05% respectively. The runoff coefficient, which represents the proportion of precipitation that becomes runoff, follows a similar pattern to the glacier runoff changes. It initially increases until the turning point of glacier melting occurs, then decreases, and eventually reaches a relatively stable state after the glaciers completely melt (Fig. 11 (c)). Before the turning point, runoff coefficient is almost equal or even greater than 1. The maximum values of the runoff coefficient occur in 2021 and 2019, coinciding with the tipping points of the glacier runoff. By the end of the 21st century, the runoff coefficient is projected to be dramatically reduced to approximately 0.42. These results indicate that glacier play a key role in water resource supply.

Two hydrological phenomena observed in permafrost mountainous catchments,

475 namely the low runoff in the early thawing season (LRET) and discontinuous baseflow

476 recession (DBR) (Gao et al., 2022), are expected to persist in the future (Fig. 12).

477 Meanwhile, baseflow, which represents the sustained flow of water from groundwater,

478 shows an increasing trend. The duration of the early thawing season is projected to be

479 further reduced. The first recession coefficient remains unchanged, while the second

480 recession coefficient progressively increases. Under the SSP2-4.5 scenario, the second

481 recession coefficient is equal to 74 days, which is consistent with the recession

482 coefficient in 2060 under the SSP5-8.5 scenario. This suggests that the permafrost area

483 undergoes less significant changes under SSP2-4.5 scenario than SSP2-8.5 scenario

484 according to Figure 9. The baseflow gradually increases, especially in the SSP5-8.5

485 scenario, as indicated by the runoff depth on a logarithmic scale (Fig. 12).

486

487

488
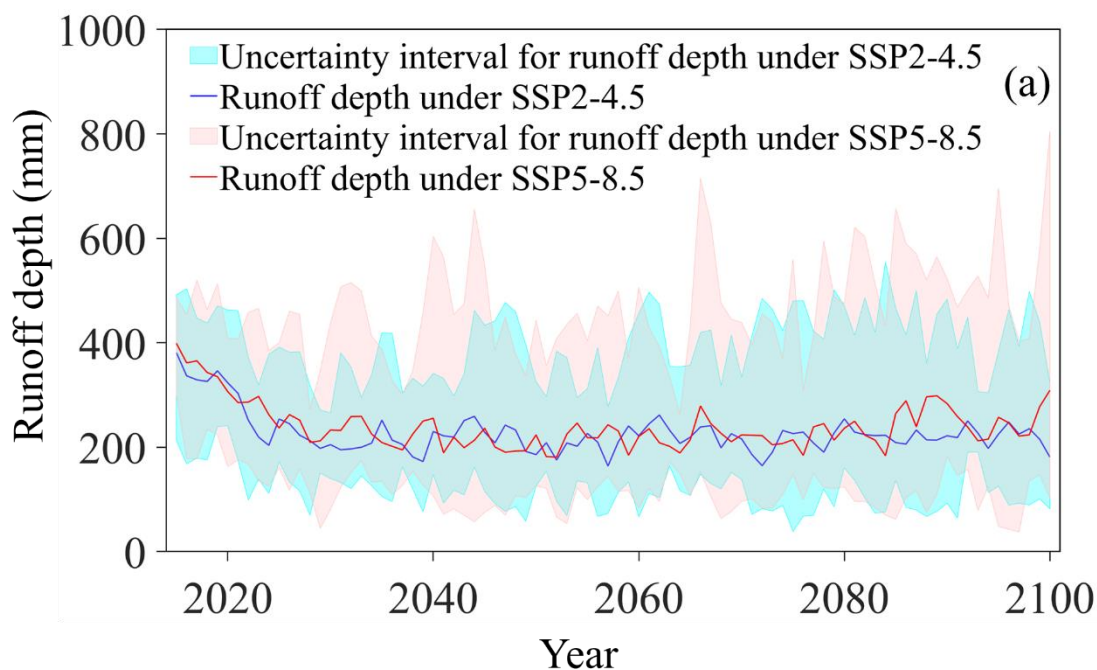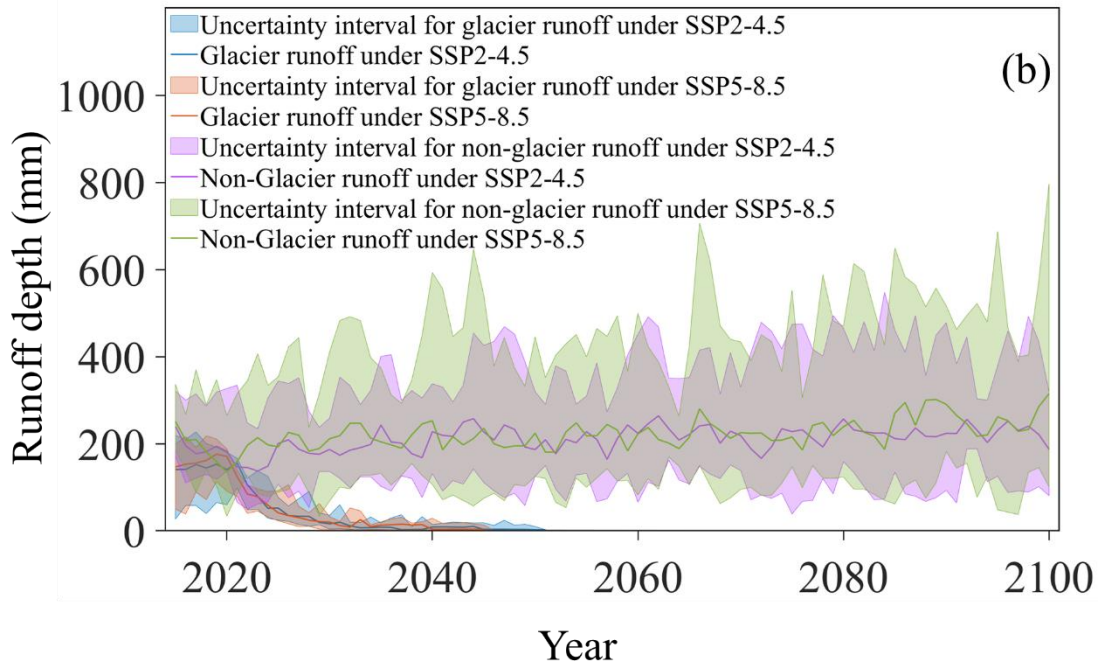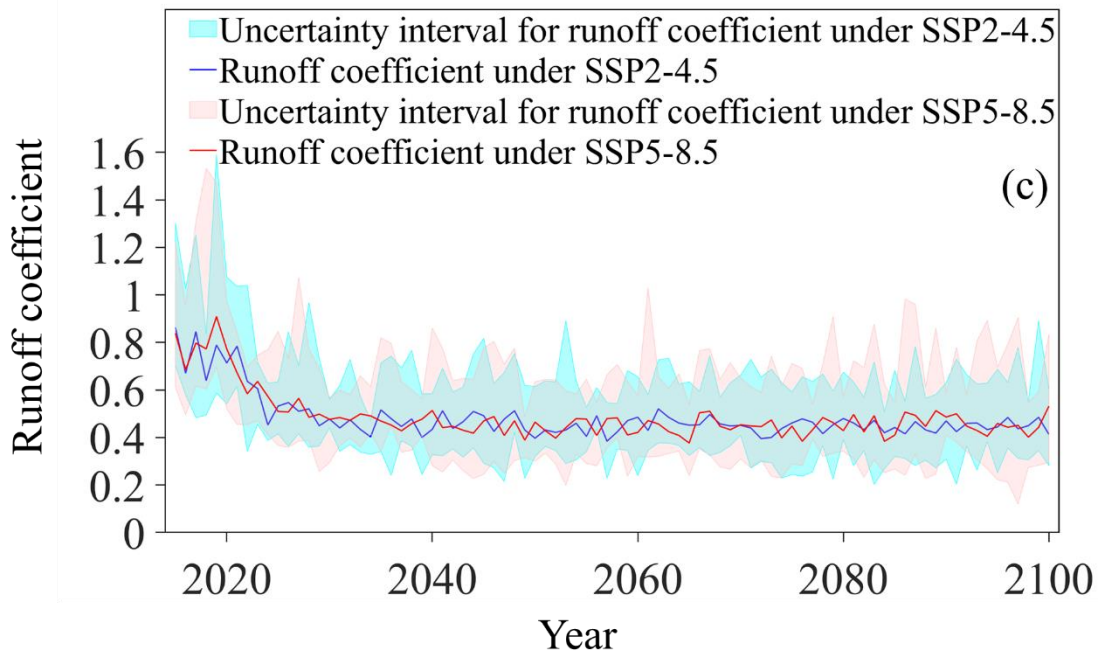
Figure 11. (a) The predicted runoff depth of the total basin. (b) Runoff in the glacier

and in the non-glacier from 2015-2100. (c) Project runoff coefficient under SSP2-4.5

and SSP5-8.5 scenarios.
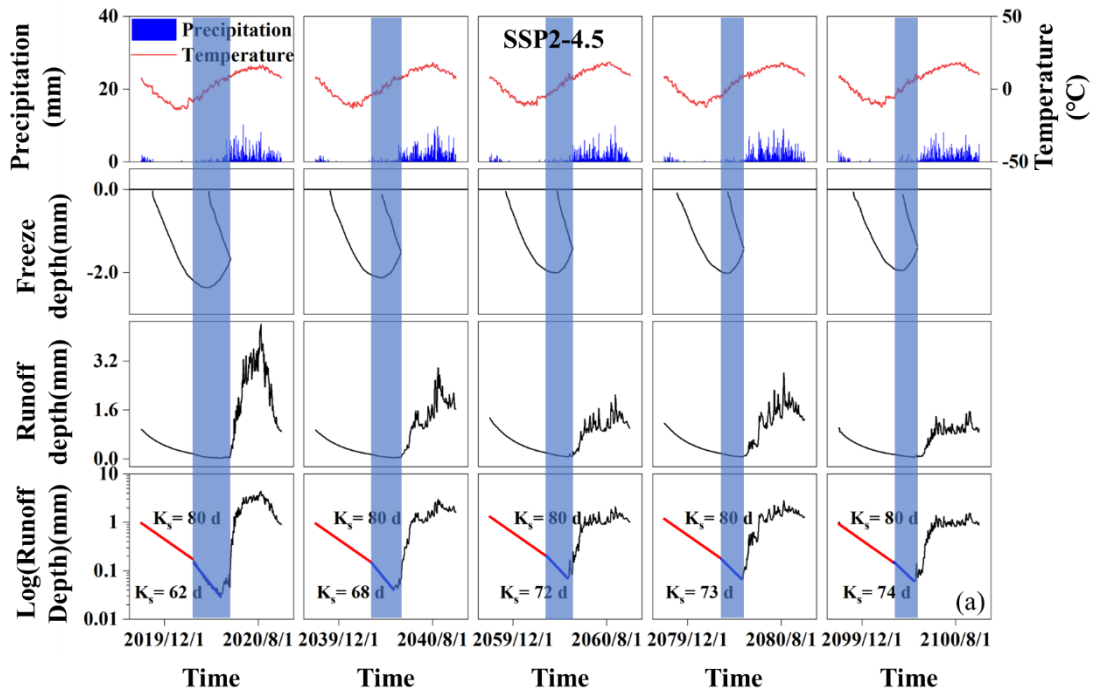
492
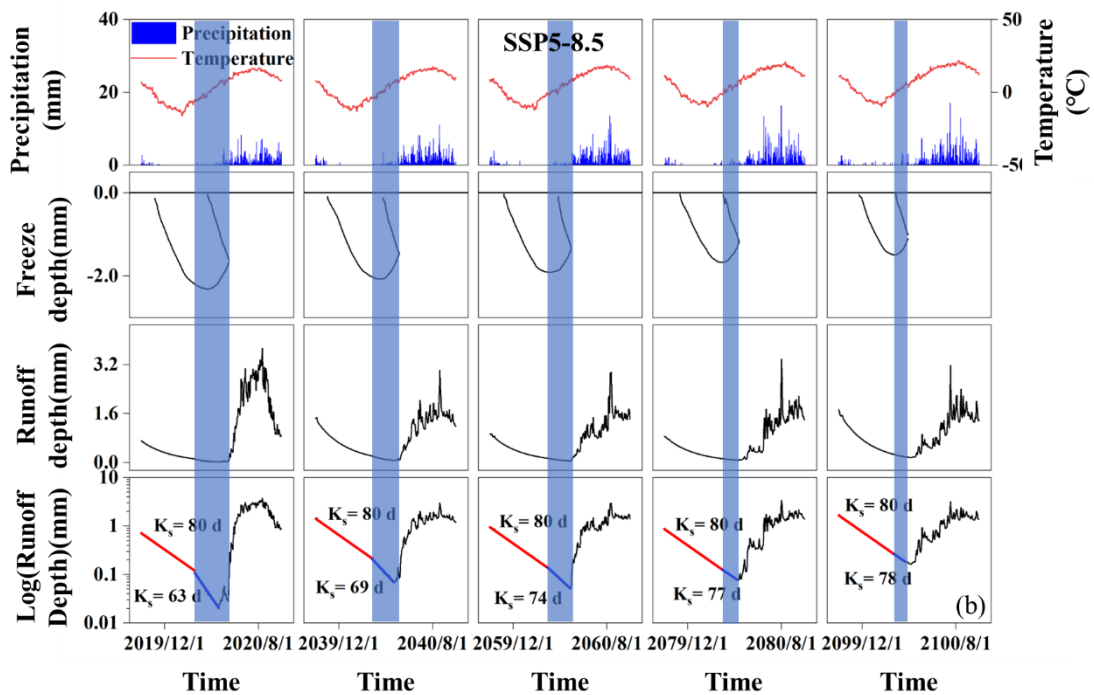
493

494   Figure 12. Temperature, precipitation, runoff depth and freeze-thaw cycle in 2020,

495   2040, 2060, 2080 and 2100 under SSP2-4.5 (a, top) and SSP5-8.5 scenarios (b, bottom).

496   **5.Discussion**

497   **5.1 The effect of the mountain cryosphere degradation on runoff**

498   Glaciers and snow are sensitive to climate change and cover play a crucial role in

499   water retention, with meltwater contributing significantly to downstream water

500   resources and the ecological environment (Stecher et al., 2023; Nan and Tian, 2024).

501   The turning point of glacier runoff represents a critical tipping point that signifies not

502   only the rapid thinning of glaciers but also the irreversible stage of water resources in

503   the basin (Brovkin et al., 2021). After the turning point the glacier thickness and glacier

504   volume rapidly decrease (Fig. 7). But the glacier thickness showed in this paper is the

505   change at the highest elevation band, which means the turning point would lag in this

506   band fort change of glacier thickness. In the Hulu catchment, the proportion of glacier

507   runoff reached 51% to 55% between 2019 and 2021, indicating that it is in the turning

508   point period (Fig. 11). Subsequently, the contribution of glacier runoff gradually

509   decreases until complete melting occurs. Temperature is the primary factor influencing

510   glacier runoff, while precipitation and temperature together determine the proportion

511   of glacier runoff in relation to total runoff. Although the highest contribution of glacier

512   runoff and the tipping point of glacier runoff may not align precisely, after the tipping

513   point, the capacity of glacier runoff to contribute to overall runoff continuously

514   diminishes. From 2015 to 2021, there has been a decreasing trend in precipitation,

515   leading to a corresponding decline in non-glacier runoff (Fig. 6 and Fig. 11). Thus,

516   while glacier runoff has increased, the total runoff has decreased. However, between

517   2032 and 2038, even though rainfall continues to decline, the contribution of glacier

518   runoff to overall runoff becomes negligible due to the limited volume of ice remaining

519   (glacier volume $< 1 \times 10^6$ m^3), resulting in minimal glacier melting runoff (Fig. 7 and

520   Fig. 11). On the other hand, once the glaciers have completely melted, the total runoff

521   in the Hulu catchment is reduced by 16% to 18%, and the runoff coefficient is halved

522   (Fig. 9 and Fig. 10). This highlights the critical role of glaciers as solid freshwater

523   reservoirs in regulating water sources and mitigating droughts (McCarthy et al., 2022).

524   The freeze-thaw cycle has a significant impact on runoff yield and hydrological

525   response routines in the Hulu catchment (Sun et al., 2022; Wang et al., 2020).

526   Precipitation in the Hulu catchment is primarily concentrated in the summer when soil

527   moisture is high and even close to saturation, making saturation excess flow the main

528   mechanism for runoff generation (Li et al., 2016). During the freeze-thaw cycle, the

529   weak permeability of frozen soil affects both surface runoff and infiltration. Soil runoff

530   primarily occurs through underground in hillslope and surface water flow in riparian

531   area, resulting in a faster response to rainfall and snowmelt and contributing to a higher

532   runoff coefficient (Hu et al., 2022; Jones et al., 2023). However, it is important to note

533   that shallow frozen soil does not completely block the interaction between deeper soil

534   layers and the surface. Frost heave in the soil creates large pores, allowing snowmelt

535   water and precipitation to bypass the matrix layer and reach the deeper soils (Jiang et

536   al., 2021; Zhang et al., 2023). This phenomenon is considered one of the significant

537   reasons for low runoff in the early thawing season (Mohammed et al., 2021). Low

538   runoff is observed between the frozen season and complete thawing season (Fig. 12).

539   The duration of freeze-thaw cycles in seasonally frozen soils is shortening, and freeze

540   onset is being delayed due to the warming climate, resulting in a decreasing duration of

541   low runoff. However, the temperature during the freezing season remains lower than

542   the initial frost heave temperature of the soil, and there is still a deficit of soil water in

543   the early thaw, indicating that the prevalence of low runoff will persist in the future

544   (Teng et al., 2022; Wen et al., 2024).

545   The freezing state has a significant impact on the recession process of baseflow,

546 and permafrost plays a crucial role in discontinuous baseflow (Cooper et al., 2023; J.

547 Wang et al., 2022). During the freezing season, baseflow follows a linear recession

548 process (K_s = 80 days), with contributions from both permafrost and seasonally frozen

549 soil regions (Fig. 12). In the frozen season, the groundwater under the supra-permafrost

550 layer becomes inactive, and baseflow is solely derived from the seasonally frozen soil

551 regions, causing a discontinuous recession. With climate warming, the lower limit of

552 permafrost gradually moves upward along the elevation, resulting in the shrinking of

553 the permafrost region. This suggests that in the future, an increased proportion of

554 baseflow will originate from the expanding area of seasonally frozen soil, leading to a

555 gradual decrease in the influence of permafrost on baseflow. Consequently, the

556 discontinuous recession of baseflow will gradually transition into a linear recession.

557 Furthermore, an increase in the thickness of the active layer enhances the soil water

558 storage capacity, contributing to a gradual rise in baseflow (Yao et al., 2021).

559 **5.2 Comparison with other studies**

560 The cryosphere, including glaciers (ice sheets), seasonal snow cover, frozen soil,

561 and permafrost, plays a vital role in storing approximately 75% of the world's

562 freshwater resources (Qin et al., 2021). Although there are some differences in the the

563 driving data and models, the trends of the cryospheric elements and runoff changes are

564 still comparable and consistent. In this study, the small glaciers are projected to

565 completely melt in the Mid-21st century, which is also reported in the other area

566 (Mukhopadhyay and Khan, 2015; Baraer et al., 2012; Schwank et al., 2014). The

567 projected maximum freeze depth of seasonally frozen soil calculated in this research is

568 5.2 cm per decade, similar to the 5.4 cm per decade predicted by Wang et al. (2018). Ni

569 et al. (2021) showed that Qinghai-Tibet Plateau permafrost is at risk of disappearance

570 based on statistical and machine learning (ML) modeling approaches. This shift in

571 regions with permafrost impacts hydrological connectivity, fostering improved

572 hydrothermal conditions that enhance vegetation growth (Han and Menzel, 2022; Jin et

573 al., 2022). Few studies have focused on the change in the snow cover days and snow

574 water equivalent in the Heihe river basin in the future, but many researches have

575 indicated that the snow-free period increases and the snow water equivalent decreases

576 due to climatic warming in Tibet Plateau (Zhang and Ma, 2018). The reduction of the

577 snow cover period may result in an earlier peak in spring snowmelt floods, thereby

578 increasing the risk of flooding (Chai et al., 2022). Simultaneously, the decrease in snow

579 water equivalent may impact plant water supply, placing pressure on ecosystems (Guan

580 et al., 2022). Although cryospheric elements have a trend of degradation in different

581 regions, the impact on runoff may differ. However, on a longer time scale, the

582 degradation of the cryosphere will lead to a decrease in runoff (Xu et al., 2024). This

583 study confirmed that runoff from cryospheric melting is one of the main factors

584 controlling runoff, and degradation of the cryosphere may exacerbate the risk of future

585 droughts.

586 **5.3 Uncertainty and limitations**

587 Uncertainty in this study comes from the GCMs, the downscaling and bias

588 correction methods, and the structure and parameters of the FLEX-Cryo model. The

589 temperature and precipitation projections from different GCMs at the basin scale

590 introduce uncertainty. Moreover, four bias correction methods were used to correct the

591 GCMs based on the observation, which may ensure consistent relative trends but not

592 improve the accuracy of precipitation and temperature frequency distribution and

593 seasonal variations. This may cause some uncertainty in the simulation results (Jia et

594   al., 2023).

595   In this research, the time-variant albedo information and the aspect are worthwhile

596   to be taken into account for improving glacier melting simulations, which require

597   further observation and quantitative studies (Arnold et al., 2006; Feng et al., 2024). The

598   change in elements is sensitive to energy. The snow cover and the effect of topographic

599   shading may also have an effect on the degradation and thus hydrologic response, which

600   warrants further investigation (Zhang, 2005). On a long time scale, the degradation of

601   frozen soil and glacier may result in thaw lake generation and other landscapes changes,

602   which may effect on the runoff yield and baseflow recession (Serban et al., 2021).

603   **6.Conclusions**

604   In this study, we employed the FLEX-Cryo model and data from eight Global

605   Climate Models (GCMs) under the SSP2-4.5 and SSP5-8.5 scenarios to predict the

606   potential impacts of climate change on the mountain cryosphere and hydrology. Results

607   from the projected change of mountain cryosphere elements, glacier, snow and frozen

608   soil are expected to undergo degradation. The glacier will completely melt by the

609   middle of the 21st century. Snow cover day will decrease by 45 and 76 days, and snow

610   water equivalent will decrease by 0.24mm/yr and 0.35mm/yr. The thaw onset is

611   expected to advance 19 days and 32 days. The active layer thickness will increase by

612   8.24cm/10yr.

613   The degradation of the mountain cryosphere has significant implications for water

614   resources. The tipping point of glacier runoff is projected to occur in the 2020s. Once

615   the glaciers have completely melted, the runoff is projected to decrease by

616   approximately 16% and 18% under the SSP2-4.5 and SSP5-8.5 scenarios, respectively.

617   Importantly, the duration of low runoff will shorten, baseflow will increase and the

618 discontinue recession of baseflow will gradually transform to a more linear pattern.

619   This study provides insights into the potential impacts of climate change on the

620 mountain cryosphere and hydrology. The projected changes in glacier retreat, snow

621 cover, and frozen soil dynamics highlight the urgent need for proactive water resource

622 management strategies in the face of a changing climate. Further modelling research

623 and monitoring efforts are necessary to refine these projections and guide effective

624 adaptation measures to sustainably manage water resources in mountainous regions.

625

626 **Competing interests**

627 At least one of the (co-)authors is a member of the editorial board of Hydrology and

628 Earth System Sciences.

629

630 **Acknowledgements**

631 This research has been supported by the National Natural Science Foundation of China

632 (grant no. 42071081 and 42122002). Zheng Duan acknowledges the support from the

633 Crafoord Foundation (No. 20210552).

634

635 **References**

636   Abdelhamed, M. S., Elshamy, M. E., Wheater, H. S., and Razavi, S.: Hydrologic-

637 land surface modelling of the Canadian sporadic-discontinuous permafrost:

638 Initialization and uncertainty propagation, Hydrol. Process., 36,

639 https://doi.org/10.1002/hyp.14509, 2022.

640   Adler, C., Huggel, C., Orlove, B., and Nolin, A.: Climate change in the mountain

641 cryosphere: impacts and responses, Reg Environ Change, 19, 1225–1228,

https://doi.org/10.1007/s10113-019-01507-6, 2019.

Andrianaki, M., Shrestha, J., Kobierska, F., Nikolaidis, N. P., and Bernasconi, S. M.: Assessment of SWAT spatial and temporal transferability for a high-altitude glacierized catchment, Hydrol. Earth Syst. Sci., 23, 3219–3232, https://doi.org/10.5194/hess-23-3219-2019, 2019.

Arendt, A., Krakauer, N., Kumar, S. V., Rounce, D. R., and Rupper, S.: Editorial: Collaborative Research to Address Changes in the Climate, Hydrology and Cryosphere of High Mountain Asia, Front. Earth Sci., 8, 605336, https://doi.org/10.3389/feart.2020.605336, 2020.

Arnold, N. S., Rees, W. G., Hodson, A. J., and Kohler, J.: Topographic controls on the surface energy balance of a high Arctic valley glacier, J. Geophys. Res., 111, 2005JF000426, https://doi.org/10.1029/2005JF000426, 2006.

Aubry-Wake, C. and Pomeroy, J. W.: Predicting Hydrological Change in an Alpine Glacierized Basin and Its Sensitivity to Landscape Evolution and Meteorological Forcings, Water Resour. Res., 59, https://doi.org/10.1029/2022WR033363, 2023.

Baraer, M., Mark, B. G., McKenzie, J. M., Condom, T., Bury, J., Huh, K.-I., Portocarrero, C., Gómez, J., and Rathay, S.: Glacier recession and water resources in Peru's Cordillera Blanca, J. Glaciol., 58, 134–150, https://doi.org/10.3189/2012JoG11J186, 2012.

Blöschl, G., Bierkens, M. F. P., Chambel, A., Cudennec, C., Destouni, G., Fiori, A., Kirchner, J. W., McDonnell, J. J., Savenije, H. H. G., Sivapalan, M., Stumpp, C., Toth, E., Volpi, E., Carr, G., Lupton, C., Salinas, J., Széles, B., Viglione, A., Aksoy, H., Allen, S. T., Amin, A., Andréassian, V., Arheimer, B., Aryal, S. K., Baker, V., Bardsley, E., Barendrecht, M. H., Bartosova, A., Batelaan, O., Berghuijs, W. R., Beven, K., Blume,

666   T., Bogaard, T., Borges De Amorim, P., Böttcher, M. E., Boulet, G., Breinl, K., Brilly,

667   M., Brocca, L., Buytaert, W., Castellarin, A., Castelletti, A., Chen, X., Chen, Y., Chen,

668   Y., Chifflard, P., Claps, P., Clark, M. P., Collins, A. L., Croke, B., Dathe, A., David, P.

669   C., De Barros, F. P. J., De Rooij, G., Di Baldassarre, G., Driscoll, J. M., Duethmann, D.,

670   Dwivedi, R., Eris, E., Farmer, W. H., Feiccabrino, J., Ferguson, G., Ferrari, E., Ferraris,

671   S., Fersch, B., Finger, D., Foglia, L., Fowler, K., Gartsman, B., Gascoin, S., Gaume, E.,

672   Gelfan, A., Geris, J., Gharari, S., Gleeson, T., Glendell, M., Gonzalez Bevacqua, A.,

673   González-Dugo, M. P., Grimaldi, S., Gupta, A. B., Guse, B., Han, D., Hannah, D.,

674   Harpold, A., Haun, S., Heal, K., Helfricht, K., Herrnegger, M., Hipsey, M., Hlaváčiková,

675   H., Hohmann, C., Holko, L., Hopkinson, C., Hrachowitz, M., Illangasekare, T. H., Inam,

676   A., Innocente, C., Istanbulluoglu, E., Jarihani, B., et al.: Twenty-three unsolved

677   problems in hydrology (UPH) – a community perspective, Hydrology. Sci. J., 64, 1141–

678   1158, https://doi.org/10.1080/02626667.2019.1620507, 2019.

679   Bolibar, J., Rabatel, A., Gouttevin, I., Zekollari, H., and Galiez, C.: Nonlinear

680   sensitivity of glacier mass balance to future climate change unveiled by deep learning,

681   Nat. Commun., 13, 409, https://doi.org/10.1038/s41467-022-28033-0, 2022.

682   Brovkin, V., Brook, E., Williams, J. W., Bathiany, S., Lenton, T. M., Barton, M.,

683   DeConto, R. M., Donges, J. F., Ganopolski, A., McManus, J., Praetorius, S., De Vernal,

684   A., Abe-Ouchi, A., Cheng, H., Claussen, M., Crucifix, M., Gallopín, G., Iglesias, V.,

685   Kaufman, D. S., Kleinen, T., Lambert, F., Van Der Leeuw, S., Liddy, H., Loutre, M.-F.,

686   McGee, D., Rehfeld, K., Rhodes, R., Seddon, A. W. R., Trauth, M. H., Vanderveken,

687   L., and Yu, Z.: Past abrupt changes, tipping points and cascading impacts in the Earth

688   system, Nat. Geosci., 14, 550–558, https://doi.org/10.1038/s41561-021-00790-5, 2021.

689   Chadburn, S. E., Burke, E. J., Cox, P. M., Friedlingstein, P., Hugelius, G., and

Westermann, S.: An observation-based constraint on permafrost loss as a function of global warming, Nature Clim. Change, 7, 340–344, https://doi.org/10.1038/nclimate3262, 2017.

Chai, C., Wang, L., Chen, D., Zhou, J., Liu, H., Zhang, J., Wang, Y., Chen, T., and Liu, R.: Future snow changes and their impact on the upstream runoff in Salween, Hydrol. Earth Syst. Sci., 26, 4657–4683, https://doi.org/10.5194/hess-26-4657-2022, 2022.

Chang, Z., Qi, P., Zhang, G., Sun, Y., Tang, X., Jiang, M., Sun, J., and Li, Z.: Latitudinal characteristics of frozen soil degradation and their response to climate change in a high-latitude water tower, CATENA, 214, 106272, https://doi.org/10.1016/j.CATENA.2022.106272, 2022.

Chen, R., Duan, K., Shang, W., Shi, P., Meng, Y., and Zhang, Z.: Increase in seasonal precipitation over the Tibetan Plateau in the 21st century projected using CMIP6 models, Atmospheric Research, 277, 106306, https://doi.org/10.1016/j.atmosres.2022.106306, 2022

Chen, R. S., Lu, S.-H., Kang, E. S., Ji, X., Zhang, Z., Yang, Y., and Qing, W.: A distributed water-heat coupled model for mountainous watershed of an inland river basin of Northwest China (I) model structure and equations, Environ. Geol., 53, 1299–1309, https://doi.org/10.1007/s00254-007-0738-2, 2008.

Connon, R. F., Chasmer, L., Haughton, E., Helbig, M., Hopkinson, C., Sonnentag, O., and Quinton, W. L.: The implications of permafrost thaw and land cover change on snow water equivalent accumulation, melt and runoff in discontinuous permafrost peatlands, Hydrol. Process., 35, e14363, https://doi.org/10.1002/hyp.14363, 2021.

Cooper, M. G., Zhou, T., Bennett, K. E., Bolton, W. R., Coon, E. T., Fleming, S.

W., Rowland, J. C., and Schwenk, J.: Detecting Permafrost Active Layer Thickness Change From Nonlinear Baseflow Recession, Water Resour. Res, 59, https://doi.org/10.1029/2022WR033154, 2023.

Cullen, N. J., Sirguey, P., Mölg, T., Kaser, G., Winkler, M., and Fitzsimons, S. J.: A century of ice retreat on Kilimanjaro: the mapping reloaded, The Cryosphere, 7, 419–431, https://doi.org/10.5194/tc-7-419-2013, 2013.

Ding, Y., Zhang, S., Zhao, L., Li, Z., and Kang, S.: Global warming weakening the inherent stability of glaciers and permafrost, Sci. Bull., 64, 245–253, https://doi.org/10.1016/j.scib.2018.12.028, 2019.

Ding, Y., Zhang, S., and Chen, R.: Cryospheric Hydrology: Decode the Largest Freshwater Reservoir on Earth, Bulletin of the Chinese Academy of Sciences, 35, 414–424, 2020.

Elshamy, M. E., Princz, D., Sapriza-Azuri, G., Abdelhamed, M. S., Pietroniro, A., Wheater, H. S., and Razavi, S.: On the configuration and initialization of a large-scale hydrological land surface model to represent permafrost, Hydrol. Earth Syst. Sci., 24, 349–379, https://doi.org/10.5194/hess-24-349-2020, 2020.

Farinotti, D., Huss, M., Fürst, J. J., Landmann, J., Machguth, H., Maussion, F., and Pandit, A.: A consensus estimate for the ice thickness distribution of all glaciers on Earth, Nat. Geosci., 12, 168–173, https://doi.org/10.1038/s41561-019-0300-3, 2019.

Feng, S., Cook, J. M., Naegeli, K., Anesio, A. M., Benning, L. G., and Tranter, M.: The Impact of Bare Ice Duration and Geo‐Topographical Factors on the Darkening of the Greenland Ice Sheet, Geophysical Research Letters, 51, e2023GL104894, https://doi.org/10.1029/2023GL104894, 2024.

Fenicia, F. and McDonnell, J. J.: Modeling streamflow variability at the regional

738 scale: (1) perceptual model development through signature analysis, J. Hydrol., 605,

739 127287, https://doi.org/10.1016/j.jhydrol.2021.127287, 2022.

740 Gao, H., Han, C., Chen, R., Feng, Z., Wang, K., Fenicia, F., and Savenije, H.:

741 Frozen soil hydrological modeling for a mountainous catchment northeast of the

742 Qinghai–Tibet Plateau, Hydrol. Earth Syst. Sci., 26, 4187–4208,

743 https://doi.org/10.5194/hess-26-4187-2022, 2022.

744 Gao, H., Feng, Z., Zhang, T., Wang, Y., He, X., Li, H., Pan, X., Ren, Z., Chen, X.,

745 Zhang, W., and Duan, Z.: Assessing glacier retreat and its impact on water resources in

746 a headwater of Yangtze River based on CMIP6 projections, Science of The Total

747 Environment, 765, 142774, https://doi.org/10.1016/j.scitotenv.2020.142774, 2021.

748 Gao, T., Kang, S., Chen, R., Zhang, T., Zhang, T., Han, C., Tripathee, L., Sillanpää,

749 M., and Zhang, Y.: Riverine dissolved organic carbon and its optical properties in a

750 permafrost region of the Upper Heihe River basin in the Northern Tibetan Plateau, Sci.

751 Total Environ., 686, 370–381, https://doi.org/10.1016/j.scitotenv.2019.05.478, 2019.

752 Gilg, O., Kovacs, K. M., Aars, J., Fort, J., Gauthier, G., Grémillet, D., Ims, R. A.,

753 Meltofte, H., Moreau, J., Post, E., Schmidt, N. M., Yannic, G., and Bollache, L.: Climate

754 change and the ecology and evolution of Arctic vertebrates, Ann. Ny. Acad. Sci., 1249,

755 166–190, https://doi.org/10.1111/j.1749-6632.2011.06412.x, 2012.

756 Giovando, J. and Niemann, J. D.: Wildfire Impacts on Snowpack Phenology in a

757 Changing Climate Within the Western U.S., Water Resour. Res., 58, e2021WR031569,

758 https://doi.org/10.1029/2021WR031569, 2022.

759 Gisnås, K., Westermann, S., Schuler, T. V., Melvold, K., and Etzelmüller, B.:

760 Small-scale variation of snow in a regional permafrost model, The Cryosphere, 10,

761 1201–1215, https://doi.org/10.5194/tc-10-1201-2016, 2016.

762   Guan, X., Guo, S., Huang, J., Shen, X., Fu, L., and Zhang, G.: Effect of seasonal

763   snow on the start of growing season of typical vegetation in Northern Hemisphere,

764   Geography   and   Sustainability,   3,   268–276,

765   https://doi.org/10.1016/j.geosus.2022.09.001, 2022.

766   Hamon, W.R.: Estimating potential evapotranspiration. J. Hydraul. Div.-ASCE 87,

767   107–120, 1961.

768   Han, L. and Menzel, L.: Hydrological variability in southern Siberia and the role

769   of   permafrost   degradation,   J.   Hydrol.,   604,   127203,

770   https://doi.org/10.1016/j.jhydrol.2021.127203, 2022.

771   He, Q., Kuang, X., Chen, J., Hao, Y., Feng, Y., Wu, P., and Zheng, C.: Glacier

772   retreat and its impact on groundwater system evolution in the Yarlung Zangbo source

773   region,   Tibetan   Plateau,   J.   Hydrol.:   Regional   Studies,   47,   101368,

774   https://doi.org/10.1016/j.ejrh.2023.101368, 2023.

775   He, Z., Duethmann, D., and Tian, F.: A meta-analysis based review of quantifying

776   the contributions of runoff components to streamflow in glacierized basins. J. Hydrol.,

777   603, 126890, https://doi.org/10.1016/j.jhydrol.2021.126890, 2021.

778   Hu, G., Li, X., Yang, X., Shi, F., Sun, H., and Cui, B.: Identifying Spatiotemporal

779   Patterns of Hillslope Subsurface Flow in an Alpine Critical Zone on the Qinghai‐

780   Tibetan Plateau Based on Three‐Year, High‐Resolution Field Observations, Water

781   Resour. Res, 58, e2022WR032098, https://doi.org/10.1029/2022WR032098, 2022.

782   Huss, M. and Fischer, M.: Sensitivity of Very Small Glaciers in the Swiss Alps to

783   Future Climate Change, Front. Earth Sci., 4, https://doi.org/10.3389/feart.2016.00034,

784   2016.

785   Huss, M. and Hock, R.: Global-scale hydrological response to future glacier mass

786   loss, Nature Clim Change, 8, 135–140, https://doi.org/10.1038/s41558-017-0049-x,

787   2018.

788   Huss, M., Jouvet, G., Farinotti, D., and Bauder, A.: Future high-mountain

789   hydrology: a new parameterization of glacier retreat, Hydrol. Earth Syst. Sci., 14, 815–

790   829, https://doi.org/10.5194/hess-14-815-2010, 2010.

791   Intergovernmental Panel On Climate Change (Ipcc): The Ocean and Cryosphere

792   in a Changing Climate: Special Report of the Intergovernmental Panel on Climate

793   Change, 1st ed., Cambridge University Press, https://doi.org/10.1017/9781009157964,

794   2022.

795   Jia, Q., Jia, H., Li, Y., and Yin, D.: Applicability of CMIP5 and CMIP6 Models in

796   China: Reproducibility of Historical Simulation and Uncertainty of Future Projection,

797   Journal of Climate, 36, 5809–5824, https://doi.org/10.1175/JCLI-D-22-0375.1, 2023.

798   Jiang, R., Li, T., Liu, D., Fu, Q., Hou, R., Li, Q., Cui, S., and Li, M.: Soil infiltration

799   characteristics and pore distribution under freezing–thawing conditions, The

800   Cryosphere, 15, 2133–2146, https://doi.org/10.5194/tc-15-2133-2021, 2021.

801   Jin, X., Jin, H., Luo, D., Sheng, Y., Wu, Q., Wu, J., Wang, W., Huang, S., Li, X.,

802   Liang, S., Wang, Q., He, R., Serban, R. D., Ma, Q., Gao, S., and Li, Y.: Impacts of

803   Permafrost Degradation on Hydrology and Vegetation in the Source Area of the Yellow

804   River on Northeastern Qinghai-Tibet Plateau, Southwest China, Front. Earth Sci., 10,

805   845824, https://doi.org/10.3389/feart.2022.845824, 2022.

806   Jones, M. W., Sebestyen, S. D., Dymond, S. F., Ng, G. H. C., and Feng, X.: Soil

807   frost controls streamflow generation processes in headwater catchments, J. Hydrol., 617,

808   https://doi.org/10.1016/j.jhydrol.2022.128801, 2023.

809   Kaplan Pastíriková, L., Hrbáček, F., Uxa, T., and Láska, K.: Permafrost table

temperature and active layer thickness variability on James Ross Island, Antarctic Peninsula, in 2004–2021, Sci. Total Environ., 869, 161690, https://doi.org/10.1016/j.scitotenv.2023.161690, 2023.

Li, L., Xu, Z., Zuo, D., and Zhao, J.: A grid-based integrated surface–groundwater model (GISMOD), J. Water Clim. Change, 7, 296–320, https://doi.org/10.2166/wcc.2015.006, 2016.

Li, X., Jin, H., Sun, L., Wang, H., Huang, Y., He, R., Chang, X., Yu, S., and Zang, S.: TTOP‑model‑based maps of permafrost distribution in Northeast China for 1961–2020, Permafrost periglac, 33, 425–435, https://doi.org/10.1002/ppp.2157, 2022.

Li, Z., Feng, Q., Chen, W., Wang, T., Cheng, Yan, G., Xiaoyan, G., Yanhui, P., Jianguo, L., Rui, G., and Bing, J.: Study on the contribution of cryosphere to runoff in the cold alpine basin: A case study of Hulugou River Basin in the Qilian Mountains, Global and Planetary Change, 122, 345–361, https://doi.org/10.1016/j.gloplacha.2014.10.001, 2014.

Liu, J. and Chen, R.: Discriminating types of precipitation in Qilian Mountains, Tibetan Plateau, Journal of Hydrology: Regional Studies, 5, 20–32, https://doi.org/10.1016/j.ejrh.2015.11.013, 2016.

Liu, Z., Cuo, L., and Sun, N.: Tracking snowmelt during hydrological surface processes using a distributed hydrological model in a mesoscale basin on the Tibetan Plateau, J. Hydrol., 616, https://doi.org/10.1016/j.jhydrol.2022.128796, 2023.

Ma, J., Li, R., Huang, Z., Wu, T., Wu, X., Zhao, L., Liu, H., Hu, G., Xiao, Y., Du, Y., Yang, S., Liu, W., Jiao, Y., and Wang, S.: Evaluation and spatio-temporal analysis of surface energy flux in permafrost regions over the Qinghai-Tibet Plateau and Arctic

using CMIP6 models, International Journal of Digital Earth, 15, 1947–1965, https://doi.org/10.1080/17538947.2022.2142307, 2022.

Martin, L. C. P., Westermann, S., Magni, M., Brun, F., Fiddes, J., Lei, Y., Kraaijenbrink, P., Mathys, T., Langer, M., Allen, S., and Immerzeel, W. W.: Recent ground thermo-hydrological changes in a southern Tibetan endorheic catchment and implications for lake level changes, Hydrol. Earth Syst. Sci., 27, 4409–4436, https://doi.org/10.5194/hess-27-4409-2023, 2023

McCarthy, M., Meier, F., Fatichi, S., Stocker, B. D., Shaw, T. E., Miles, E., Dussaillant, I., and Pellicciotti, F.: Glacier Contributions to River Discharge During the Current Chilean Megadrought, Earth's Future, 10, e2022EF002852, https://doi.org/10.1029/2022EF002852, 2022.

Michel, A., Schaefli, B., Wever, N., Zekollari, H., Lehning, M., and Huwald, H.: Future water temperature of rivers in Switzerland under climate change investigated with physics-based models, Hydrol. Earth Syst. Sci., 26, 1063–1087, https://doi.org/10.5194/hess-26-1063-2022, 2022.

Miner, K., Turetsky, M., Malina, E., Bartsch, A., Tamminen, J., McGuire, A., Fix, A., Sweeney, C., Elder, C., and Miller, C.: Permafrost carbon emissions in a changing Arctic, Nature Reviews Earth & Environmental, 3, 55–67, https://doi.org/10.1038/s43017-021-00230-3, 2022.

Mohammed, A. A., Cey, E. E., Hayashi, M., and Callaghan, M., V.: Simulating preferential flow and snowmelt partitioning in seasonally frozen hillslopes, Hydrol. Process., 35, https://doi.org/10.1002/hyp.14277, 2021.

Moreno, P. I., Fercovic, E. I., Soteres, R. L., Ugalde, P. I., Sagredo, E. A., and Villa-Martínez, R. P.: Glacier and terrestrial ecosystem evolution in the Chilotan

858 archipelago sector of northwestern Patagonia since the Last Glacial Termination, Earth-

859 Science Reviews, 235, 104240, https://doi.org/10.1016/j.earscirev.2022.104240, 2022.

860 Mukhopadhyay, B. and Khan, A.: A reevaluation of the snowmelt and glacial melt

861 in river flows within Upper Indus Basin and its significance in a changing climate,

862 Journal of Hydrology, 527, 119–132, https://doi.org/10.1016/j.jhydrol.2015.04.045,

863 2015.

864 Nan, Y. and Tian, F.: Glaciers determine the sensitivity of hydrological processes

865 to perturbed climate in a large mountainous basin on the Tibetan Plateau, Hydrol. Earth

866 Syst. Sci., 28, 669–689, https://doi.org/10.5194/hess-28-669-2024, 2024.

867 Negi, V. S., Tiwari, D. C., Singh, L., Thakur, S., and Bhatt, I. D.: Review and

868 synthesis of climate change studies in the Himalayan region, Environ Dev Sustain, 24,

869 10471–10502, https://doi.org/10.1007/s10668-021-01880-5, 2022.

870 Ni, J., Wu, T., Zhu, X., Hu, G., Zou, D., Wu, X., Li, R., Xie, C., Qiao, Y., Pang, Q.,

871 Hao, J., and Yang, C.: Simulation of the Present and Future Projection of Permafrost on

872 the Qinghai‑Tibet Plateau with Statistical and Machine Learning Models, JGR

873 Atmospheres, 126, e2020JD033402, https://doi.org/10.1029/2020JD033402, 2021.

874 Nury, A. H., Sharma, A., Mehrotra, R., Marshall, L., and Cordery, I.: Projected

875 Changes in the Tibetan Plateau Snowpack Resulting From Rising Global Temperatures,

876 J. Geophy Res.-Atmos. , 127, https://doi.org/10.1029/2021JD036201, 2022.

877 Peng, Z., Tian, F., Wu, J., Huang, J., Hu, H., and Darnault, C. J. G.: A numerical

878 model for water and heat transport in freezing soils with nonequilibrium ice‑water

879 interfaces, Water Resources Research, 52, 7366‑7381,

880 https://doi.org/10.1002/2016WR019116, 2016.

881 Pomeroy, J. W., Brown, T., Fang, X., Shook, K. R., Pradhananga, D., Armstrong,

882 R., Harder, P., Marsh, C., Costa, D., Krogh, S. A., Aubry-Wake, C., Annand, H.,

883 Lawford, P., He, Z., Kompanizare, M., and Lopez Moreno, J. I.: The cold regions

884 hydrological modelling platform for hydrological diagnosis and prediction based on

885 process understanding, J. Hydrol., 615, 128711,

886 https://doi.org/10.1016/j.jhydrol.2022.128711, 2022.

887 Pothula, S. K. and Adams, B. J.: Community assembly in the wake of glacial

888 retreat: A meta‐analysis, Glob. Chang Biol, 28, 6973–6991,

889 https://doi.org/10.1111/gcb.16427, 2022.

890 Qin, D., Yao, T., Ding, Y., and Ren, J.: Classification and Geographical

891 Distribution of Cryosphere, in: Introduction to Cryospheric Science. Springer

892 Singapore, Singapore, 33–79, https://doi.org/10.1007/978-981-16-6425-0_2, 2021.

893 Rabatel, A., Ceballos, J. L., Micheletti, N., Jordan, E., Braitmeier, M., González,

894 J., Mölg, N., Ménégoz, M., Huggel, C., and Zemp, M.: Toward an imminent extinction

895 of Colombian glaciers?, Geografiska Annaler: Series A, Phys Geog, 100, 75–95,

896 https://doi.org/10.1080/04353676.2017.1383015, 2018.

897 Ragettli, S., Immerzeel, W. W., and Pellicciotti, F.: Contrasting climate change

898 impact on river flows from high-altitude catchments in the Himalayan and Andes

899 Mountains, Proc. Natl. Acad. Sci. U.S.A., 113, 9222–9227,

900 https://doi.org/10.1073/pnas.1606526113, 2016.

901 Rasul, G., Pasakhala, B., Mishra, A., and Pant, S.: Adaptation to mountain

902 cryosphere change: issues and challenges, Clim Dev, 12, 297–309,

903 https://doi.org/10.1080/17565529.2019.1617099, 2020.

904 Rosier, S. H. R., Reese, R., Donges, J. F., De Rydt, J., Gudmundsson, G. H., and

905 Winkelmann, R.: The tipping points and early warning indicators for Pine Island Glacier,

West Antarctica, The Cryosphere, 15, 1501–1516, https://doi.org/10.5194/tc-15-1501-2021, 2021.

Schwank, J., Escobar, R., Girón, G. H., and Morán-Tejeda, E.: Modeling of the Mendoza river watershed as a tool to study climate change impacts on water availability, Environmental Science & Policy, 43, 91–97, https://doi.org/10.1016/j.envsci.2014.01.002, 2014.

Serban, R., Jin, H., Serban, M., and Luo, D.: Shrinking thermokarst lakes and ponds on the northeastern Qinghai-Tibet plateau over the past three decades, PERMAFROST AND PERIGLACIAL PROCESSES, 32, 601–617, https://doi.org/10.1002/ppp.2127, 2021.

Stecher, G., Hohensinner, S., and Herrnegger, M.: Changes in the water retention of mountainous landscapes since the 1820s in the Austrian Alps, Front. Environ. Sci., 11, 1219030, https://doi.org/10.3389/fenvs.2023.1219030, 2023.

Sun, B., Liu, J., Ren, F., Li, H., Zhang, G., Ma, J., Ma, B., and Li, Z.: Effects of seasonal freeze–thaw and wind erosion on runoff and sediment yields of three loamy slopes of Loess Plateau, China, CATENA, 215, 106309, https://doi.org/10.1016/j.catena.2022.106309, 2022.

Tang, G., Clark, M. P., Knoben, W. J. M., Liu, H., Gharari, S., Arnal, L., Beck, H. E., Wood, A. W., Newman, A. J., and Papalexiou, S. M.: The Impact of Meteorological Forcing Uncertainty on Hydrological Modeling: A Global Analysis of Cryosphere Basins, Water Resour. Res, 59, e2022WR033767, https://doi.org/10.1029/2022WR033767, 2023.

Teng, J., Liu, J., Zhang, S., and Sheng, D.: Frost heave in coarse-grained soils: experimental evidence and numerical modelling, GEOTECHNIQUE, 73, 1100–1111,

930 https://doi.org/10.1680/jgeot.21.00182, 2022.

931 Teutschbein, C. and Seibert, J.: Bias correction of regional climate model

932 simulations for hydrological climate-change impact studies: Review and evaluation of

933 different methods, J. Hydrol., 456–457, 12–29,

934 https://doi.org/10.1016/j.jhydrol.2012.05.052, 2012.

935 Van Der Geest, K. and Van Den Berg, R.: Slow-onset events: a review of the

936 evidence from the IPCC Special Reports on Land, Oceans and Cryosphere, CURR

937 OPIN ENV SUST, 50, 109–120, https://doi.org/10.1016/j.cosust.2021.03.008, 2021.

938 Vincent, C. and Thibert, E.: Brief communication: Non-linear sensitivity of glacier

939 mass balance to climate attested by temperature-index models, The Cryosphere, 17,

940 1989–1995, https://doi.org/10.5194/tc-17-1989-2023, 2023.

941 Wang, J., Chen, X., Gao, M., Hu, Q., and Liu, J.: Changes in nonlinearity and

942 stability of streamflow recession characteristics under climate warming in a large

943 glaciated basin of the Tibetan Plateau, Hydrol. Earth Syst. Sci., 26, 3901–3920,

944 https://doi.org/10.5194/hess-26-3901-2022, 2022a.

945 Wang, K., Zhang, T., and Clow, G. D.: Permafrost Thermal Responses to

946 Asymmetrical Climate Changes: An Integrated Perspective, Geophys. Res. Lett., 50,

947 e2022GL100327, https://doi.org/10.1029/2022GL100327, 2023.

948 Wang, Q., Qi, J., Wu, H., Zeng, Y., Shui, W., Zeng, J., and Zhang, X.: Freeze-Thaw

949 cycle representation alters response of watershed hydrology to future climate change,

950 CATENA, 195, https://doi.org/10.1016/j.catena.2020.104767, 2020.

951 Wang, S., Yang, Y., and Che, Y.: Global Snow- and Ice-Related Disaster Risk: A

952 Review, Nat. Hazards Rev., 23, 03122002, https://doi.org/10.1061/(ASCE)NH.1527-

953 6996.0000584, 2022b.

954 Wang, X., Chen, R., Liu, G., Yang, Y., Song, Y., Liu, J., Liu, Z., Han, C., Liu, X.,

955 Guo, S., Wang, L., and Zheng, Q.: Spatial distributions and temporal variations of the

956 near-surface soil freeze state across China under climate change, Global Planetary

957 Change, 172, 150–158, https://doi.org/10.1016/j.gloplacha.2018.09.016, 2019.

958 Wang, Y., Yang, H., Gao, B., Wang, T., Qin, Y., and Yang, D.: Frozen ground

959 degradation may reduce future runoff in the headwaters of an inland river on the

960 northeastern Tibetan Plateau, J. Hydrol., 564, 1153–1164,

961 https://doi.org/10.1016/j.jhydrol.2018.07.078, 2018.

962 Wei, L., Zhao, W., Feng, X., Han, C., Li, T., Qi, J., and Li, Y.: Freeze-thaw

963 desertification of alpine meadow in Qilian Mountains and the implications for alpine

964 ecosystem management, CATENA, 232, 107471,

965 https://doi.org/10.1016/j.catena.2023.107471, 2023.

966 Wen, Y., Liu, B., Jiang, H., Li, T.-Y., Zhang, B., and Wu, W.: Initial soil moisture

967 prewinter affects the freeze–thaw profile dynamics of a Mollisol in Northeast China,

968 CATENA, 234, 107648, https://doi.org/10.1016/j.catena.2023.107648, 2024.

969 Wiersma, P., Aerts, J., Zekollari, H., Hrachowitz, M., Drost, N., Huss, M.,

970 Sutanudjaja, E. H., and Hut, R.: Coupling a global glacier model to a global

971 hydrological model prevents underestimation of glacier runoff, Hydrol. Earth Syst. Sci.,

972 26, 5971–5986, https://doi.org/10.5194/hess-26-5971-2022, 2022.

973 Xing, Z. P., Zhao, L., Fan, L., Hu, G. J., Zou, D. F., Wang, C., Liu, S. C., Du, E. J.,

974 Xiao, Y., Li, R., Liu, G. Y., Qiao, Y. P., and Shi, J. Z.: Changes in the ground surface

975 temperature in permafrost regions along the Qinghai–Tibet engineering corridor from

976 1900 to 2014: A modified assessment of CMIP6, Advances in Climate Change Research,

977 14, 85–96, https://doi.org/10.1016/j.accre.2023.01.007, 2023.

978   Xu, P., Yan, D., Weng, B., Bian, J., Wu, C., and Wang, H.: Evolution trends and

979 driving factors of groundwater storage, recharge, and discharge in the Qinghai-Tibet

980 Plateau: Study progress and challenges, Journal of Hydrology, 631, 130815,

981 https://doi.org/10.1016/j.jhydrol.2024.130815, 2024.

982   Yang, M., Li, Z., Anjum, M. N., Kayastha, R., Kayastha, R. B., Rai, M., Zhang,

983 X., and Xu, C.: Projection of Streamflow Changes Under CMIP6 Scenarios in the

984 Urumqi River Head Watershed, Tianshan Mountain, China, Front. Earth Sci., 10,

985 857854, https://doi.org/10.3389/feart.2022.857854, 2022.

986   Yao, T., Bolch, T., Chen, D., Gao, J., Immerzeel, W., Piao, S., Su, F., Thompson,

987 L., Wada, Y., Wang, L., Wang, T., Wu, G., Xu, B., Yang, W., Zhang, G., Zhao, P., 2022.

988 The imbalance of the Asian water tower. NATURE REVIEWS EARTH &

989 ENVIRONMENT 3, 618–632. https://doi.org/10.1038/s43017-022-00299-4

990   Yao, Y., Zheng, C., Andrews, C. B., Scanlon, B. R., Kuang, X., Zeng, Z., Jeong,

991 S.-J., Lancia, M., Wu, Y., and Li, G.: Role of Groundwater in Sustaining Northern

992 Himalayan Rivers, Geophys. Res. Lett., 48, https://doi.org/10.1029/2020GL092354,

993 2021.

994   Yin, G.-A., Niu, F.-J., Lin, Z.-J., Luo, J., and Liu, M.-H.: Data-driven

995 spatiotemporal projections of shallow permafrost based on CMIP6 across the Qinghai–

996 Tibet Plateau at 1 km2 scale, Advances in Climate Change Research, 12, 814–827,

997 https://doi.org/10.1016/j.accre.2021.08.009, 2021

998   Zekollari, H., Huss, M., Farinotti, D., and Lhermitte, S.: Ice‐Dynamical Glacier

999 Evolution Modeling—A Review, Reviews of Geophysics, 60, e2021RG000754,

1000 https://doi.org/10.1029/2021RG000754, 2022.

1001   Zhang, T.: Influence of the seasonal snow cover on the ground thermal regime: An

1002 overview, Reviews of Geophysics, 43, 2004RG000157,

1003 https://doi.org/10.1029/2004RG000157, 2005.

1004 Zhang, S., Gao, X., Zhang, X., and Hagemann, S.: Projection of glacier runoff in

1005 Yarkant River basin and Beida River basin, Western China, Hydrol. Process., 26, 2773–

1006 2781, https://doi.org/10.1002/hyp.8373, 2012.

1007 Zhang, T., Li, D., and Lu, X.: Response of runoff components to climate change

1008 in the source-region of the Yellow River on the Tibetan plateau, Hydrol. Process., 36,

1009 https://doi.org/10.1002/hyp.14633, 2022.

1010 Zhang, Z., Wang, Y., Ma, Z., and Lv, M.: Response mechanism of soil structural

1011 heterogeneity in permafrost active layer to freeze-thaw action and vegetation

1012 degradation, CATENA, 230, https://doi.org/10.1016/j.catena.2023.107250, 2023.

1013 Zhang, Y. and Ma, N.: Spatiotemporal variability of snow cover and snow water

1014 equivalent in the last three decades over Eurasia, Journal of Hydrology, 559, 238–251,

1015 https://doi.org/10.1016/j.jhydrol.2018.02.031, 2018.

1016 Zhu, Y. Y. and Yang, S.: Evaluation of CMIP6 for historical temperature and

1017 precipitation over the Tibetan Plateau and its comparison with CMIP5, Advances in

1018 Climate Change Research, 11, 239–251, https://doi.org/10.1016/j.accre.2020.08.001,

1019 2020.